The effect of rotation speed and flow rate on evacuation of particles from a spinning dry powder inhaler capsule

Athiya Azeem[1], Gajendra Singh[2], Hak-Kim Chan[3], Runyu Yang[4], Shaokoon Cheng[5], and Agisilaos Kourmatzis[1]

[1]School of Aerospace, Mechanical and Mechatronic Engineering. The University of Sydney, NSW 2006, Australia
[2]School of Engineering, IIT Mandi, HP 175075, India
[3]School of Pharmacy, the University of Sydney, NSW 2006, Australia
[4]School of Material Science and Engineering, UNSW Sydney, NSW 2052, Australia
[5]School of Engineering, Macquarie University, NSW 2109, Australia

30th October 2024

Abstract

This study investigated a capsule's powder evacuation behaviour when rotating about its minor axis in a cross flow and considering the effects of rotation speed and flow rate on powder emission. The experimental platform, an optically accessible capsule chamber, was designed to uncover the independent effects of these variables by enabling high-speed imaging of the powder evacuation.

The capsules were rotated at three speeds (1500, 2500 and 3650 RPM) and two constant flow rates, 30 SLPM and 60 SLPM (inlet velocity: 16.67 m/s and 33.33 m/s, respectively). Two powders were selected: a lactose carrier, Respitose (SV010, D50 = 104 µm) and Mannitol (D50 = 7 µm), the latter representing pure active pharmaceutical ingredient formulations that form agglomerates. In addition to imaging, the capsule was weighed before and after each device actuation to quantify powder emission.

Increasing the flow rate was found to have the largest impact on the mass emitted from the capsule at all rotation speeds. The emitted mass for all cases was highly variable and influenced by the cohesiveness of the powder and subsequent blockage of the capsule aperture. The potential for blockage was more pronounced for mannitol at the high rotation speeds. Emitted dose over time was modelled using a natural logarithm function to describe the rate of emptying and demonstrate the advantage of increased flow rate and favourability of low/-moderate rotation speeds. The study of powder size distribution during evacuation found no significant difference between flow conditions for mannitol, as dispersion was dominated by shearing at the capsule aperture.

1 Introduction

Dry powder inhalers (DPI) are used to manage a variety of chronic obstructive pulmonary diseases (COPD) and asthma. Pulmonary drug delivery has been an active area of research due to the targeted delivery and improved bioavailability that has useful therapeutic benefits for respiratory diseases (Claus et al. 2014). Despite their widespread use, performance of these devices concerning the degree of powder dispersion and proportion of lung delivery (Islam and Cleary 2012) can vary between and within patients. This variability can be attributed to a number of factors including inhaler design, patient inhalation profiles and powder formulation (Newman and Busse 2002).

A key challenge of dry powder inhalation is the dispersion and de-agglomeration of drug powder to achieve an mean particle diameter conducive to pulmonary deposition. The mechanical design of the inhaler devices can be critical to achieving this such as by minimizing deposition in the upper airway (Islam and Cleary 2012). As DPIs become more common and the hopes of expanding their applications are being explored, there is an increased need to define optimal inhaler design configurations (Chaurasiya and Zhao 2020).

Current commercial devices typically leverage a combination of different mechanisms and designs to deliver the desired powder deposition. At this time there is a fundamental lack in the understanding of how each of these confounding variables impact flow behaviour and the subsequent device performance characteristics. As a result there is a need for studies that not only vary single design element in a complex commercial device but also isolate specific mechanism in simplified geometries to better understand the effect of different design elements. A key impediment to further developing efficacious commercial devices is the use of well validated CFD models with confidence. As there are challenges with modelling variable axis of rotation capsules within DPIs, provision of a detailed experimental account of powder dynamics from a fixed axis of rotation capsule can serve to act as a useful data set for model validation.Therefore, the simplifications made to this experiment are intentional, and there to aid in the understand of a particular fundamental mechanism that drives powder evacuation, that of capsule rotation

One common DPI design is a capsule-based concept where the powder is evacuated and dispersed by the patient's inspiratory effort. In these commercially available devices drug powder is loaded in the capsule. The powders are emitted through holes at the end of the capsule, and interaction between the airflow and powders is achieved by either aligning the major axis of the capsule with the airflow (e.g. Handihaler), or by rotating the capsule in a swirl chamber (e.g. Aerolizer ®, Osmohaler®or RS01 variants) (Martinelli et al. 2015).

While there is a substantial body of research on understanding these capsule-based inhalers (Lavorini, Pistolesi and Usmani 2017; Ding et al. 2021), there remains a significant degree of uncertainty around the underlying fluid mechanics that drive their performance due to their inherently complex design (Almeida et al. 2022). One study investigated the effect of capsule motion and location of piercing in several commercial DPIs including the Aerolizer, RS01 (both rotation about minor axis), Handihaler and Turbospin (both airflow inline with capsule) (Martinelli et al. 2015). The results of the study found that a spinning capsule was the most effective mechanism to improve powder emission and dispersion, whereas the piercing effect was more pronounced for carrier mixtures than for carrier-free powders (insulin) due to their high flowability. The study also noted the importance of capsule motion on emission, with the airflow being largely re-

sponsible for deagglomeration effects. Another 2011 study utilised laser diffraction particle sizing to explore the kinetics of powder emission in three different capsule-based inhalers, the Handihaler Aerolizer and Monodose Inhaler(Behara et al. 2011). This study used real-time sizing and concentration data to analyse powder emission and aerosol concentration vs time. Between these devices, the variability in powder emission was attributed to the capsule behaviour and movement. The Monodose inhaler had the most consistent evacuation and this was attributed to a more repeatable spinning motion in the device. A critical issue that needs to be resolved is that in commercial inhalers, several emptying mechanisms act simultaneously, making isolating and understanding the true cause of different evacuation characteristics challenging.

The examination of capsule motion in various commercial devices by comparing the different piercing configurations (Martinelli et al. 2015) also stated that performance would favour rotation about the minor axis with holes at the extremities compared to inhalers with axial flow evacuation.To date a majority of studies on capsule motion have been conducted with commercial devices and as a result, few have been conducted to isolate the mechanisms and their effect on capsule evacuation. This is particularly consequential for computational studies of devices with minor axis rotation such as the Aerolizer, Monodose Inhaler and RS01, which typically assume fixed axis rotation(Coates et al. 2005; Benque and Khinast 2019; Shur et al. 2012). This assumption neglects the non- uniform motion that results in a variable rotational axis which is responsible for capsule- wall collisions. For instance, for the Aerolizer, the collision behaviour of a capsule was quantified (Benque and Khinast 2019) using high speed microscopic imaging of the capsule chamber. The study found a significant deviation from the ”ideal” fixed axis rotation assumption previous simulations had implemented.

This study presents a comprehensive experimental investigation and detailed analysis of the powder dynamics from a rotating capsule. This study aims to discover the fundamental effects of combined rotation and flow on powder evacuation from an actively rotating capsule.Unlike commercial devices where various mechanisms within the inhaler design lead to compounding effects, the experimental platform presented here enables control of the rotation mechanism, independent of the flow rate, to elucidate the underlying interactions between capsule rotation and the surrounding airflow. The experimental platform is intentionally simple to enable the investigation of the mechanics of powder evacuation with well-defined boundary conditions.

This work aims to provide data to inform future design of commercial devices. By understanding if capsule rotation with respect to air flow could be modified to improve powder evacuation and deagglomeration. In commercial DPIs this can be achieved through changes in resistance or other designs elements to produce advantageous results.

2 Methodology

2.1 Platform Design

The testing platform for this study was an optically accessible channel designed to facilitate imaging of the internal geometry. The centre of the channel features a circular chamber with a diameter of 20 mm containing a platform that rotates about a fixed axis, as shown in Figure 1. The rotating platform features an indentation allowing a size 4 capsule to be affixed to the surface to ensure limited capsule movement. The capsule size was chosen to be similar to and compatible

with previous testing platforms (Singh, Tang et al. 2022).

This channel was not designed to emulate the complex geometry of commercial devices directly but aimed at producing a fundamental testing platform to study the combined effects of capsule rotation in a cross-flow.By considering fixed axis rotation, the confounding effects of capsule collisions can be removed therefore facilitating a greater understanding of a singular design element in isolation. A simplified geometry was conceived where the flow was predominantly two-dimensional. Without the axial outlet and the additional complexities of commercial inhaler devices, the simplified design allows for ease of imaging and computational model validation. The single inlet and single outlet of 5 mm wide by 6 mm tall channels were chosen where the length would enable the flow to be fully developed at the region of interest.

The resistance of the testing platform is $0.030\text{kPa}^{0.5}/\text{LPM}$ which is comparable to the Aerolizer which is used as the benchmark for rotation speed selection in this study.

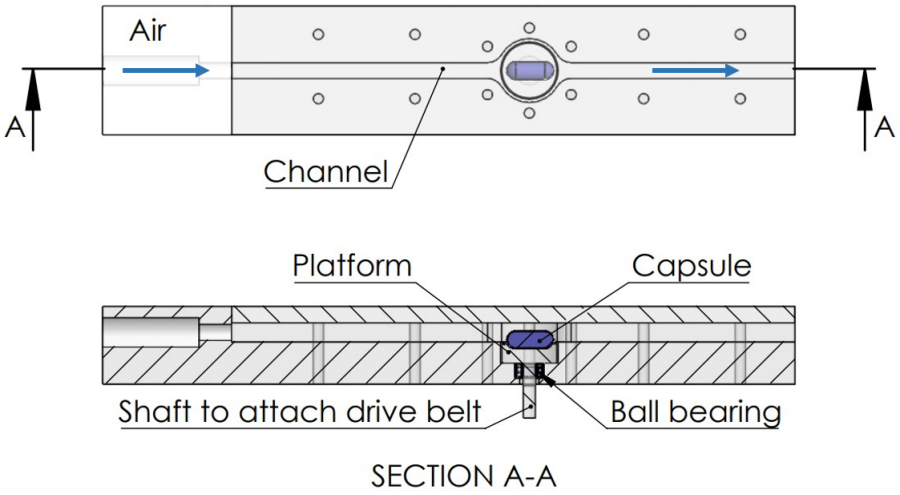

Figure 1: Testing platform

2.2 Rotation Mechanism

The bottom of the platform in the circular chamber features a shaft that connects to a motor via a drive belt/ pulley system. The motor speed was set using an L289N motor driver module and Arduino, controlled by a LabVIEW Virtual Instrument (VI). The VI was designed to simultaneously actuate the air supply, motor, and high-speed camera. The speed of the platform's rotation was monitored by the VI in real-time using a laser diode and receiver whose path would be interrupted by a 3D-printed paddle attached to the shaft of the rotating platform (see Figure 2). Details on this rotation speed measurement system can be found in Appendix C.

Using the above system, the rotation speeds obtained are shown in Figure C.18, for 3 repetitions in each setting (Low, Medium and High). This demonstrates the variation in rotation speed for each setting and their consistency between repetitions. As can be noted from Figure C.18, motors do not begin spinning at their target speed immediately but progress through a small period of acceleration. This would also be present in devices that use passive rotation speed however, these real time measurements allow those periods to be quantified.

2.3 Powder Selection

Two powders were used in this study; a lactose carrier, Respitose ®(SV010) from DFE Pharma and spray-dried mannitol following the process outlined in previous studies (Singh, Tang et al. 2022).

In previous studies, several samples of mannitol were selected at varying average diameters, usually 3, 5 and 7 µm, to test the effects of agglomeration that would be present in different pharmaceutical formulations (Azeem et al. 2023). However, our preliminary testing showed that the agglomerates formed from 3 µm and 5 µm of mannitol were too cohesive to adequately evacuate the chamber under the examined conditions. The 7-micron sample maintained a consistent presence of agglomerates but was less susceptible to blocking the capsule aperture than samples of smaller constituent sizes. Powder size of this sample was 7 μm where $d_{50} = 6.92\mu m$ and a span of 1.28 μm. The reader should note that this sizing is for the powder constituent size and not the pre-dispersed powder. While this would be useful, the sizing of mannitol within the capsule is highly variable. Quantifying this variability would require substantial additional measurements beyond the scope of this study. However, previous work by these authors (A. Lowe et al. 2021) has demonstrated a detailed classification of the fragmentation dynamics of mannitol agglomerates, which was subsequently used as the basis for validating a robust computational model (Li et al. 2022). Whilst the agglomerates in the study by Lowe at al were large (1mm), the data was successfully used to validate a more general DEM-CFD model approach that could form the basis for future work to examine the influence of the initial agglomerate population size within a capsule on its subsequent dispersion behaviour.

The specific lactose carrier was chosen as it does not agglomerate and can demonstrate evacuation behaviour independent of cohesive forces between powder particles. Without agglomeration, SV010 is also suitable for calibration of particle sizing done via high-speed imaging by comparing size distribution obtained via laser diffraction with the size measurements from the binarized images. Laser diffraction measurements were taken with a the Malvern Master Sizer 2000, where particle size was found to be $d_{50} = 104\mu m$ and a span of $1.68\mu m$ as stated in previous works (Azeem et al. 2023).

Powder selection was made in line with previous works, which emphasise investigation of powder dynamics with respect to particle constituent size. As a result, no carrier blends were utilised in this study but should be considered in future works to link these findings to commercial blends. Further information about the spray drying process and storage conditions can be found in Appendix A.1.

2.4 Imaging

High-speed back-lit imaging was used to take particle size and velocity measurements as described extensively in previous work (Azeem et al. 2023)(Singh, Albyn Lowe et al. 2021). To obtain microscopic images, a VC-Photron FASTCAM mini AX100 (Tokyo, Japan) high-speed camera was used with a Questar QM-100 microscope lens used in conjunction with an Oxford Lasers FIREFLY 300 W double-pulsed laser as the light source.With this equipment and the positioning of the camera relative to the channel, a field of view (FOV) of 3.8 mm wide and 2.6 mm tall could be achieved with a resolution of 768 X 528 pixels. The location of this FOV is shown in Figure 2 and was chosen to be in the channel, 5mm downstream from the capsule tip when the aperture

is aligned with the flow. This allows for the characterisation of the powder as it exits the capsule, unlike previous studies that consider emission behaviour from the device as a whole, where flow effects would compound on capsule behaviour.

The plane of focus was aligned at the centre of the channel with a 80 μm depth of field achieved by the microscopic lens. Images were acquired at a rate if 10,000 frames per second.

Further details about the imaging apparatus and schematic can be found in Appendix A.2

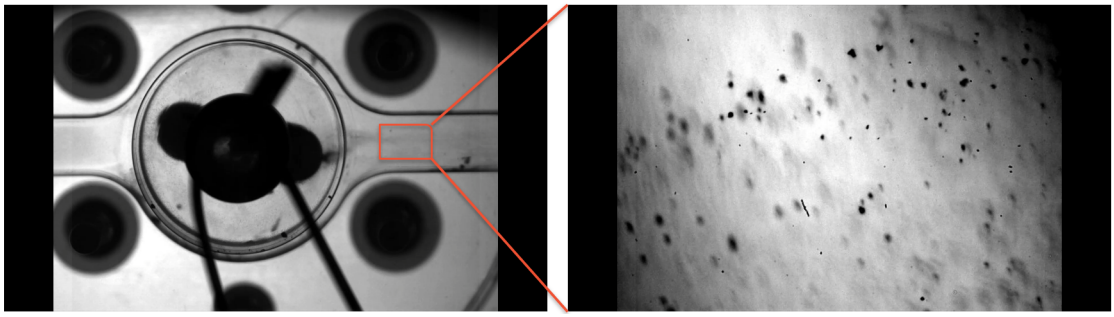

Figure 2: Field of View for Microscopic Imaging of capsule evacuation behaviour

2.5 Experimental Procedure

In order to better understand the evacuation behaviour of a capsule under these highly controlled conditions, high-speed imaging of the whole capsule in the circular chamber and microscopic imaging 5 mm downstream of the capsule were conducted. Before each actuation of the device, a capsule was loaded with 25 mg $\pm$ 0.5 mg and pierced with a single needle at both ends of the capsule using a 1.5 mm needle from the Osmohaler device. Capsules were weighed using a Radwag Analytical Balance (AS 310.R2 PLUS) with a resolution of 0.1 mg. The capsule was then carefully removed to ensure minimal powder was lost. The capsule was then inspected to ensure there were no cracks or damage to the capsule beyond the two intentionally placed holes on either end. The capsule could then be adhered to the groove on the rotating platform using a thin removable adhesive. To ensure that powder did not (or only minimally) evacuate before rotation had begun, the capsule was oriented such that the pieced holes where perpendicular to the oncoming airflow.

The flow device was actuated for three seconds using the aforementioned VI which simultaneously triggers the cross-flow and capsule rotation. The capsule was subject to a variety of flow/rotation conditions as outlined in Table 1. The airflow was controlled using an Alicat mass flow meter to set a constant flow rate of either 30 standard litres per minute (SLPM) (16.67 m/s inlet velocity and Re = 5520) or 60 SLPM (33.33 m/s inlet velocity and Re = 11040).Once the flow is enabled, the air flow reaches steady state within 0.3 seconds and average time for powder evacuation to cease was 1.5 seconds. However due to slight delay in motor rotation, the acceleration of the flow usually occurs before or just as the capsule begins to rotate. The capsule's starting orientation perpendicular to the oncoming flow further minimised exposure to the accelerating flow before rotation began.

For both flow rates, three steady-state rotation speeds of approximately 1500, 2500 and 3650 RPM were chosen, hereafter referred as Low, Medium and High speed settings. These values

were based off the linear relationship between air velocity and rotation speed (Coates et al. 2005) in the Aerolizer where a size 4 capsule that spins at approximately 2500 RPM at 60 SLPM became the medium speed for this experiment. For active rotation, an angular velocity greater than and lower than this middle value was chosen for further investigation. The exact speed of the motor was subject to mild fluctuations of approximately 65 RPM of the steady state value.

For each actuation of the device, the powder was weighed before and after to measure the amount of powder emitted from the capsule. To gain a qualitative understanding of powder evacuation behaviour, macroscopic images of the capsule were taken. The tests were conducted in triplicate for the microscopic imaging downstream of the capsule. No microscopic images were taken for the no flow case as powder would deposit in the FOV and collect obscuring any measurements that could be taken.

Other experiments that were conducted include holding the capsule stationary and inline with the oncoming airflow and rotating the capsule in the circular chamber without any cross-flow, both of which were performed to isolate the mechanisms relating flow rate and capsule rotation. For further clarity, Table 1 outlines the full experimental test matrix followed for this study, summarizing the range of capsule rotational speeds, air flow-rates, and types of measurements conducted for each case. Each experimental case shown in the table was done for both Mannitol and SV010.

Table 1: Experimental Matrix repeated for both Mannitol and SV010 evacuated over 3 second device actuation.

Flow rate	Rotation Speed Setting			
	None 0	Low ∼1500 RPM	Medium ∼2500 RPM	High ∼3600 RPM
0 SLPM (no flow case)	X	MA (2) EM(3)	MA (2) EM(3)	MA (2) EM(3)
30 SLPM, Inlet Velocity = 16.67 m/s Re = 5520	MA (2) EM(3)	MA(2) MS(3) EM(5)	MA(2) MS(3) EM(5)	MA(2) MS(3) EM(5)
60 SLPM, Inlet Velocity = 33.33 m/s Re = 11040	MA (2) EM(3)	MA(2) MS(3) EM(5)	MA(2) MS(3) EM(5)	MA(2) MS(3) EM(5)

Where X = No cases, MA = macroscopic imaging, MS = microscopic imaging, EM = emitted mass measurements. The number in bracket denotes the number of repetitions per measurement for each powder.

2.6 Image Processing

The time dependent evacuation of the powder could be monitored by analysing the changes to pixel intensity due to the attenuation of light due to powder obscuring the FOV. As the light from the laser is attenuated by the powder particles in the FOV, the overall pixel intensity drops as shown in Figure 3. The value for overall pixel intensity was taken as the summation of the intensity for all the pixels in a given frame minus the summation of the background intensity. This value was then inverted such that the peaks reflect the presence of particles and normalised to

allow for comparison between different cases where slight changes in illumination might result in fluctuation of the overall pixel intensity. For the mannitol cases, wall deposition was especially prevalent, and as a result the background intensity would decrease over the evacuation time window. To compensate for this, a moving mean was subtracted from the final signal such that any peak in the signal indicates powder visibility. Further details on the signal processing to achieve a normalised signal shown in Figure 3b can be found in Appendix D.

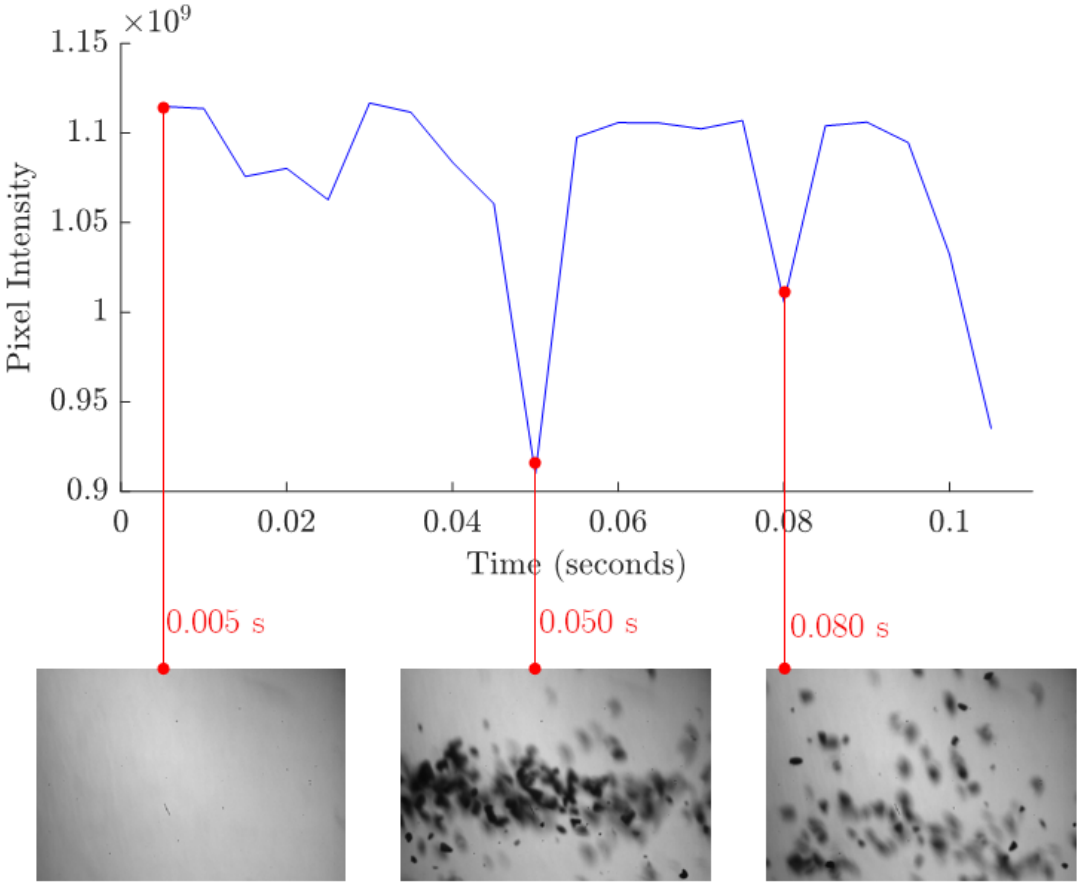

(a) Total pixel intensity over time signal

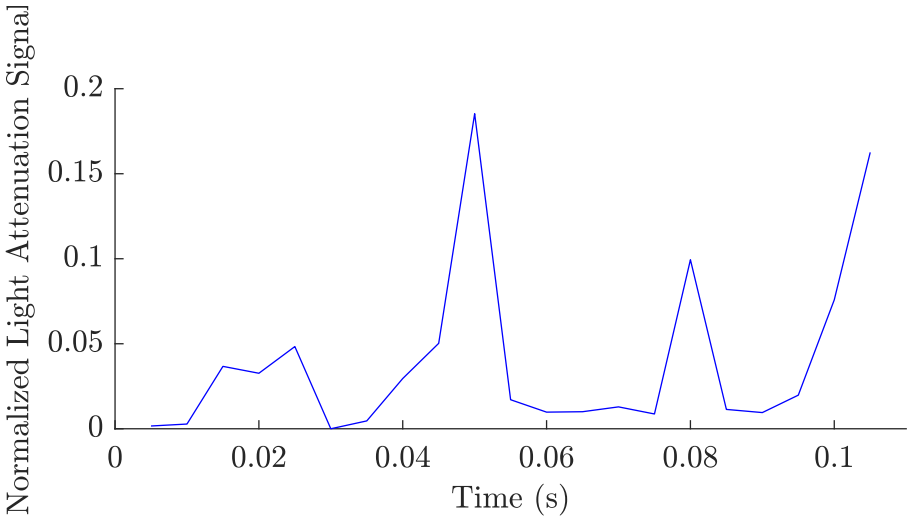

(b) Normalized signal convert to represent the amount of light attenuated

Figure 3: Sample Pixel intensity time series

2.7 Statistical Analysis

When comparing different cases, a difference in the measured parameters was deemed *significantly* different when a T-test was conducted and returned a p-value less than 0.05. Two sample T-tests were conducted in Microsoft Excel.

3 Results and Discussion

3.1 Qualitative Analysis

A qualitative assessment of the powder evacuation behaviour was conducted using the macroscopic images of the testing platform. To describe how powder evacuation occurs as the capsule rotates, the capsule chamber was segmented into six sections labelled 1-6 as shown in Figure 4.

The two powders used in this experiment exhibited different evacuation behaviours, which is likely related to their difference in size and cohesive qualities (Goh, Heng and Liew 2018). Their qualitative evacuation behaviour is discussed below.

The first notable characteristic was that evacuation commenced immediately following capsule rotation for both powders, and during the acceleration phase, before the capsule reached the predetermined steady state rotation speed.As mentioned in Section 2.5 the air flow would also be accelerating however reaches steady state before the capsule rotation achieves its maximum.

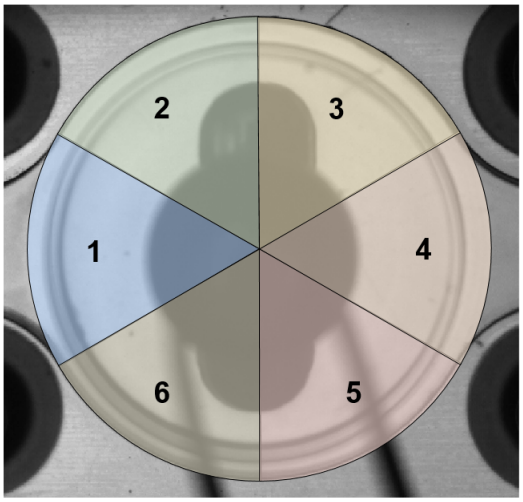

Figure 4: Capsule chamber in six segments for qualitative discussion.

3.1.1 Mannitol

Figure 5 shows key features of the evacuation process for Mannitol. At 30SLPM, a low rotation speed allowed for evacuation in segments 2-6; however, most powder evacuated in segment 4 when the capsule aligned with the airflow. Evacuation in the remaining segments only occurred in the initial rotations of the capsule (i.e. up until a speed of 1000 RPM) while most of the powder was still within the capsule. Once the initial evacuation occurred, the remaining powder was evacuated almost exclusively in segment 4. During this initial evacuation, the mass of powder emitted

is unpredictable with near identical orientations of the capsule producing different powder evacuation behaviour such as at time 0.330sec and 0.355 sec in Figure 5. This difference could be a result of the accelerating capsule and the corresponding impact on the internal powder arrangement.

At 60SLPM; evacuation occurred across the same segments (2-6), and so the full figure is not shown in this section for brevity, however the reader can observe the evacuation in segments 2 and 6 in the Appendix in Figure B.17. Generally, the obvious disparities observed for powder evacuation between segments was related to the flow rate and whether the capsule was aligned with the airflow. At 60 SLPM a much more prominent stream of particles was observed exiting the capsule, as shown in Figure 6 and this effect was present at all rotation speeds.

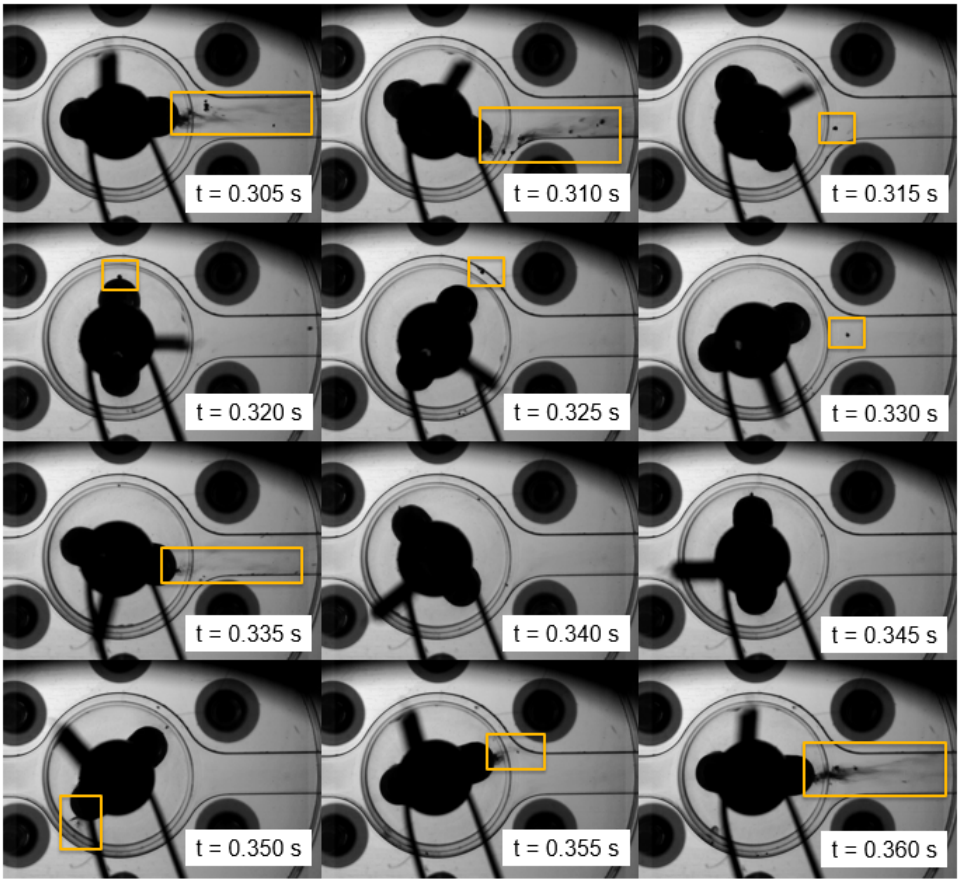

Figure 5: Macroscopic Imaging of Mannitol evacuation from capsule with low rotation speed and 30 SLPM.

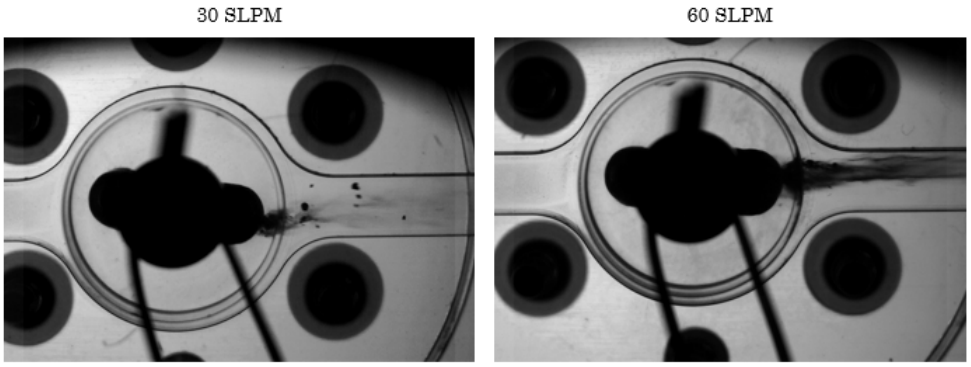

Figure 6: Mannitol in-line evacuation at 30 SLPM (Left) and 60SLPM (Right) at approx. 1500 RPM.

When increasing the rotation speed, the most notable change in the evacuation behaviour is apparent in segment 4 during capsule-flow alignment which is visible through Figure 7. For a constant flow rate, increasing the rotation speed drastically decreases the intensity of the powder burst, which is usually apparent for a capsule when rotated to segment 4. This burst is visible for the low rotation speed but is notably weaker and appears to delay such that evacuation only becomes obvious in segment 5 for the medium RPM case. At the high RPM setting, this is diminished further, as shown in Figure 7.

This behaviour can be understood by considering the aperture exposure time to the oncoming flow for each given rotational cycle.While aligned with the flow, the capsule experiences a pressure difference between both openings; aided by the resulting vacuum as a result of airflow around the capsule, powder evacuation occurs. While the internal dynamics of the capsule cannot be determined from these images, it is hypothesised that the prolonged exposure to the oncoming air gives the powder inside time to mobilise and evacuate at lower rotation speeds. By the time the powder has mobilised in the higher rotation speed cases, the capsule is no longer aligned with the flow, and evacuation briefly occurs in segment 5. Further experimental studies into the internal capsule powder dynamics are needed.

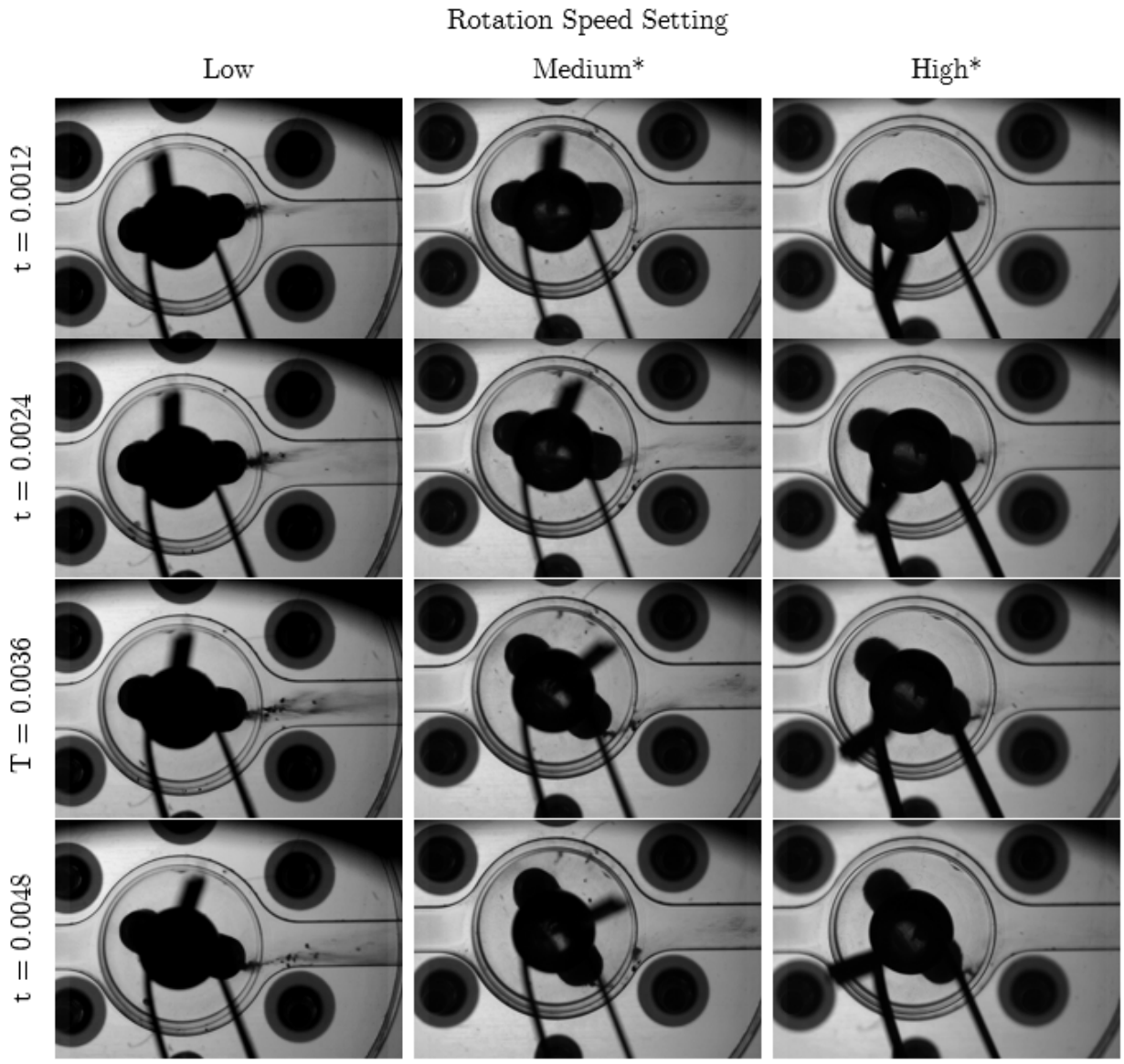

Figure 7: Mannitol Evacuation at 30SLPM when capsule is inline with cross flow. *capsule still accelerating.

3.1.2 SV010 Evacuation

Evacuation of the lactose Carrier from the capsule followed the same evacuation behaviour driven by the capsule alignment to the oncoming flow. In addition, due to the lack of cohesiveness of the SV010 particles, the powder can evacuate more continuously, in contrast to Mannitol, which agglomerates. Like with mannitol, SV010 evacuation only occurs from one end of the capsule at a time when exposed to a cross flow.

At low rotation speeds, the powder evacuation begins in segment 2, and as the capsule aligns vertically (between segment 2 and 3), the evacuation transits completely to the other end of the capsule at segment 6. Finally, when the capsule aligns longitudinally with the flow, evacuation occurs in sector 4.

At higher rotation speeds, the powder evacuation occurs from both ends and consistent evacuation is maintained at 60SLPM. This is dissimilar to mannitol where evacuation at 60SLPM was mostly limited to segment 4.

3.2 Emitted Mass Measurements

3.2.1 Rotation and Cross flow

Mannitol

Total powder emission was calculated by measuring capsule weight before and after actu- ation of the testing platform. Figure 8a shows the total percentage of loaded mannitol evacuated at the average steady-state rotation speed for each instance of powder evacuation. Increasing the flow rate positively affected capsule evacuation by forcing out larger agglomerates that would otherwise not be able to exit. From Figure 8a a high degree of variation in the total emitted mass between repetitions is evident, even under the same experimental conditions. This inconsistency between repetitions of each test case is hypothesised to result from the internal powder arrangement within the capsule and powder agglomeration. Considerations were made to investigate the potential influence of capsule acceleration on total mass emitted; however, no trend was observed.

For a given flow rate, the rotational speed was found to have a significant effect on powder discharge when comparing large changes in RPM; such as between the low and high speed cases. At both flow rates, mannitol evacuation was only shown to improve significantly when changes in the rotation speed were more than approximately 2000 RPM as shown in Figure 12.

Previous works have emphasised the importance of centrifugal force on powder evacuation (Martinelli et al. 2015). However, as observed in Figure 8a, cohesive powders may be more prone to blockage and hindered mass emission when subjected to high rotational speed. This is due to the centrifugal force pushing large amounts of the loaded powder to the pierced ends and packing them over the aperture before evacuation can occur.

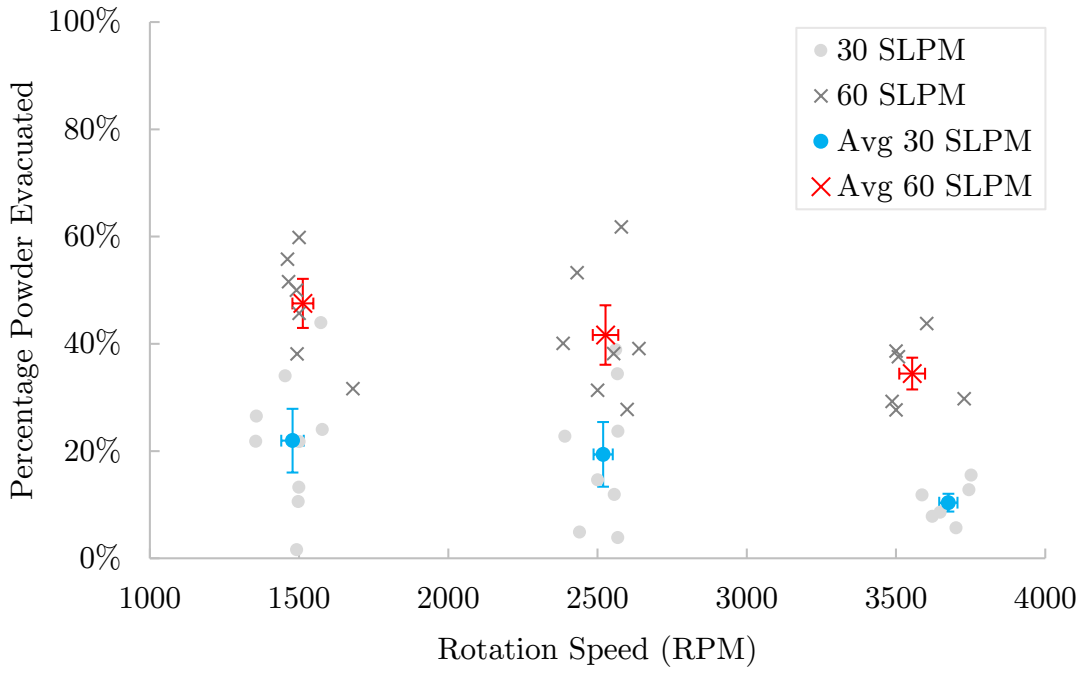

(a) Mannitol

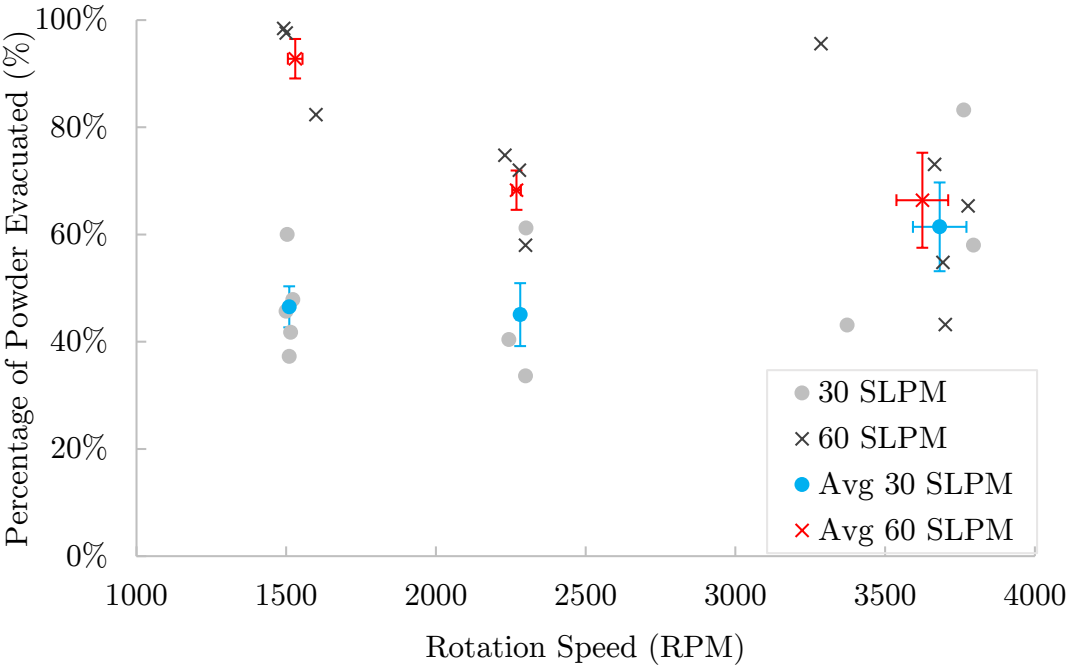

(b) Carrier (SV010)

Figure 8: Powder evacuation for given flow rate and rotation speed

Due to the significant variation between repetitions in the mannitol cases of combined air flow and rotation, additional tests were conducted to understand the evacuation of powder under each of these independent conditions. Firstly the capsule was held stationary with the aperture aligned

with the cross flow. This maximises the airflow through the capsule and denotes the optimal no-rotation case. Figure 9 shows the average powder evacuation for all cases for mannitol. When a capsule is held stationary at both flow rates the difference in evacuation is not significantly different from any of the rotation speed settings. This is again due to the high degree of variability between repetitions even without the potential for variation in rotation fluctuation or acceleration.

The second test consisted of capsule rotation without a cross-flow where centrifugal forces would purely drive emission. For each respective rotation speed the centrifugal force alone still under performs when compared to those same rotation speeds with a 60SLPM cross flow. However when comparing emission due purely to rotation (without cross flow) with cases where flow rate is 30SLPM and with rotation, a variety of results were apparent depending on rotation speed. At the low rotation speed the powder emission was significantly lower when relying purely on centrifugal force, compared to the same rotation with a 30SLPM cross flow as seen in Figure 9. The converse was true at the high rotation speed setting where evacuation was significantly higher without the 30SLPM cross flow. By comparing highspeed images of both cases it was observed that without the cross flow the powder was free to evacuate from both ends of the capsule without pressure from the oncoming air blocking the aperture in segment 1. As a result, the higher rotation speed is able to evacuate more; however, when air is introduced, this back pressure on the capsule as the powder is pushed towards the aperture by centrifugal force worsens the blockage. At lower rotation speeds, the build-up of cohesive agglomerates over the perforation was observed to be less dense than it was at high RPMs where the centrifugal forces are higher, and the cross-flow is better able to overcome this blockage. This is consistent with DEM simulations (conducted by Zhu et. al(Zhu et al. 2023)) where powder inside the capsule during rotation. shows the powder being forced toward the aperture during rotation.

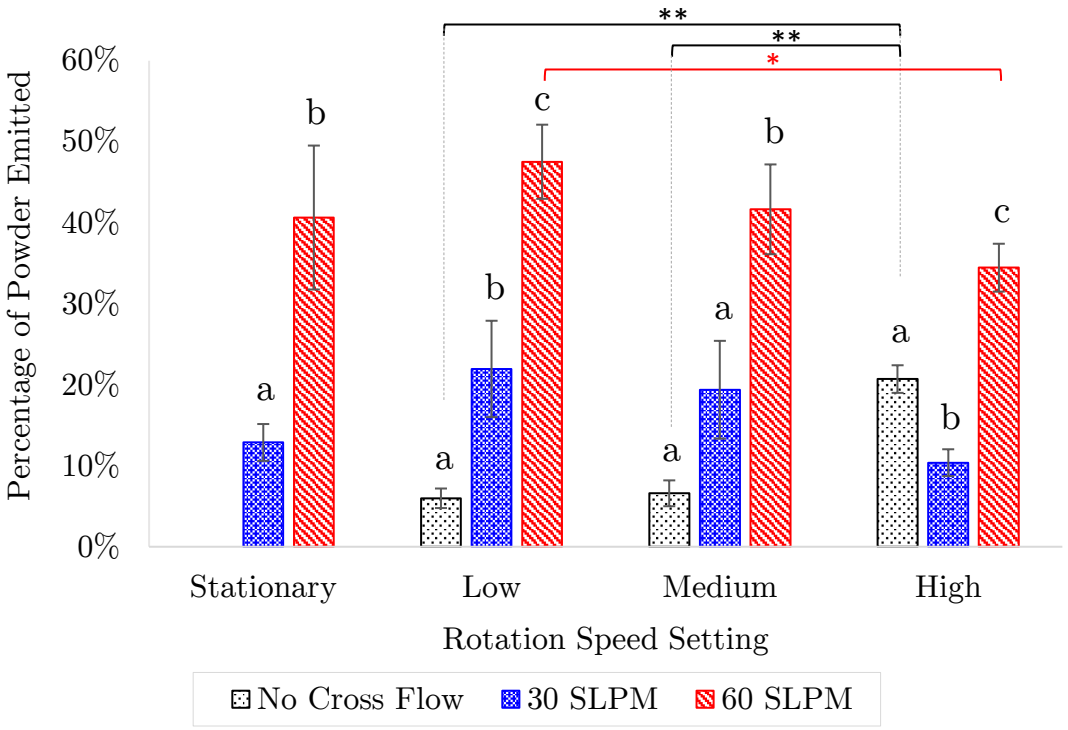

Figure 9: Mannitol evacuation with and without cross flow or rotation.* denotes $p < 0.05$, ** denotes $p < 0.01$

Carrier Formulation SV010
The degree of powder emission from a capsule was also investigated in the case of a coarser, less cohesive lactose carrier. Overall evacuation is improved for this powder compared to the more cohesive mannitol for both flow rates and rotation speeds.

There was a significant improvement in evacuation at 60 SLPM compared to 30 SLPM at the low and medium RPM settings as seen in Figure 8*b*. At a higher rotation speed of approximately 3600 RPM, the higher flow rate effect is immediately diminished, and higher variability in the emitted dose (around 10%) is observed.

The rotation speed of the carrier had no significant effect on the emission at 30 SLPM. However, when the flow rate was increased to 60SLPM, the Low RPM case showed significant superiority in powder emission, evidenced by the gap in data points shown in Figure 8b. In this configuration, it appears that evacuation mechanics were not dominated by the centrifugal force, and the cross-flow had a more pronounced effect.

At the highest RPM setting, SV010 does not experience the same diminishing evacuation performance demonstrated by mannitol especially at 30 SLPM as shown in Figure 8a. Due to a lack of agglomerates or strong cohesive forces between the lactose carrier, SV010 is able to continuously evacuate even at high rotation speeds. Therefore the improvement in evacuation in the 60 SLPM low rotation speed cases compared to high, is likely due to the increased capsule alignment time not due to aperture blockage at high rotation as was seen with mannitol.

3.3 Pixel Intensity over Time

An analysis of the fluctuations due to light attenuation from powder obstructing the light through the field of view was conducted further to quantify powder evacuation consistency under various experimental conditions. The chosen FOV is downstream of the capsule at a point of intersection for powder entering the channel from the top and bottom of the swirl chamber and directly from the capsule itself.

Light attenuation time series signals were obtained following the procedure in Section 2.6 (further details in Appendix D). For both powders, there was a high degree of variability in the signal itself, with the only common feature being occasional peaks suggesting intermittency of the powder evacuation (as shown in Figure 10), which is consistent with qualitative observations. No repeatable features were observed to distinguish particle flow conditions for a particular powder. This was expected especially for mannitol and is consistent with observations of high variability in literature (Huynh et al. 2015). Periodic analysis of these time series were conducted and found intermittency of evacuation to be consistent with rotation speed as observed qualitatively. Further details of periodic analysis can be found in Appendix E.0.1.

From this data, the approximate evacuation duration could be obtained by measuring the time at which the signal dissipated. This was characterised by the point in time when 90% of the total integral of the time series was reached, since minor variation could extend the full signal time measurement.

Mannitol was found to have both highly variable dose amounts (as stated in Section 3.2) and evacuation duration as shown in Figure 11. Due to this variability, no significant difference between flow conditions could be identified.

For SV010 at 30 SLPM, the highest rotation speed significantly reduced the evacuation duration compared to the low and medium settings as shown in Figure 11. At the low rotation speed, increasing the flow rate decreased the duration of evacuation slightly. In contrast, increasing the flow rate from 30 to 60 SLPM at a high rotation speed prolonged the evacuation. At the low rotation speed, the increase in flow rate encourages faster evacuation, thus reaching its evacuation equilibrium quickly. For the higher rotation speed, evacuation is drawn out due to less exposure time to the oncoming flow.

By comparing the evacuation duration of SV010 and mannitol a greater understanding of how powder cohesion affects capsule evacuation can be obtained. Figure 11 highlights the difference in evacuation duration between the two powders, showing that a significant difference is only observed at 30 SLPM. This suggests that at 60 SLPM, the flow rate dominates evacuation characteristics, whereas, at 30 SLPM, evacuation is more greatly affected by the powder properties and rotation effects. At the low and medium RPM setting, SV010 evacuates for a longer period of time than mannitol; however, at the highest RPM setting, the SV010 evacuation period is shorter than it is for mannitol. The average evacuation time for mannitol remains approximately constant for the changing rotation speed, and therefore, the relative difference between SV010 and mannitol evacuation time is a result of the change in SV010's evacuation behaviour. Since SV010 rarely agglomerates, it can continue flowing out even when covering the aperture. In this case, the increased rotation speed can assist in the mass evacuation. The difference this continuous flow of particles makes on evacuation and subsequent light attenuation can be seen in Figure 10 where mannitol has far more irregular peaks. The full sample time series for Mannitol and SV010, where the data of Figure 11 was extracted from, are given in the Appendix, in Figures E.23 and E.22 respectively.

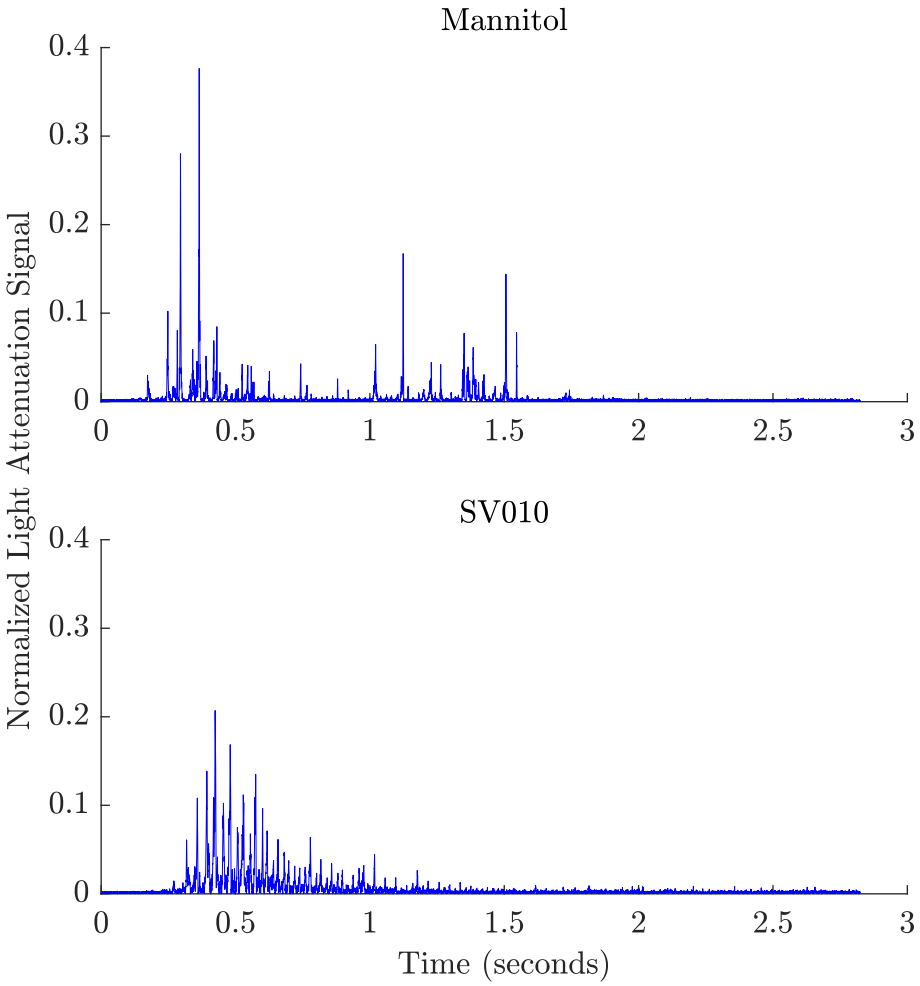

Figure 10: Light Attenuation signal for powder evacuation from capsule at 30SLPM low rotation speed for both powders.

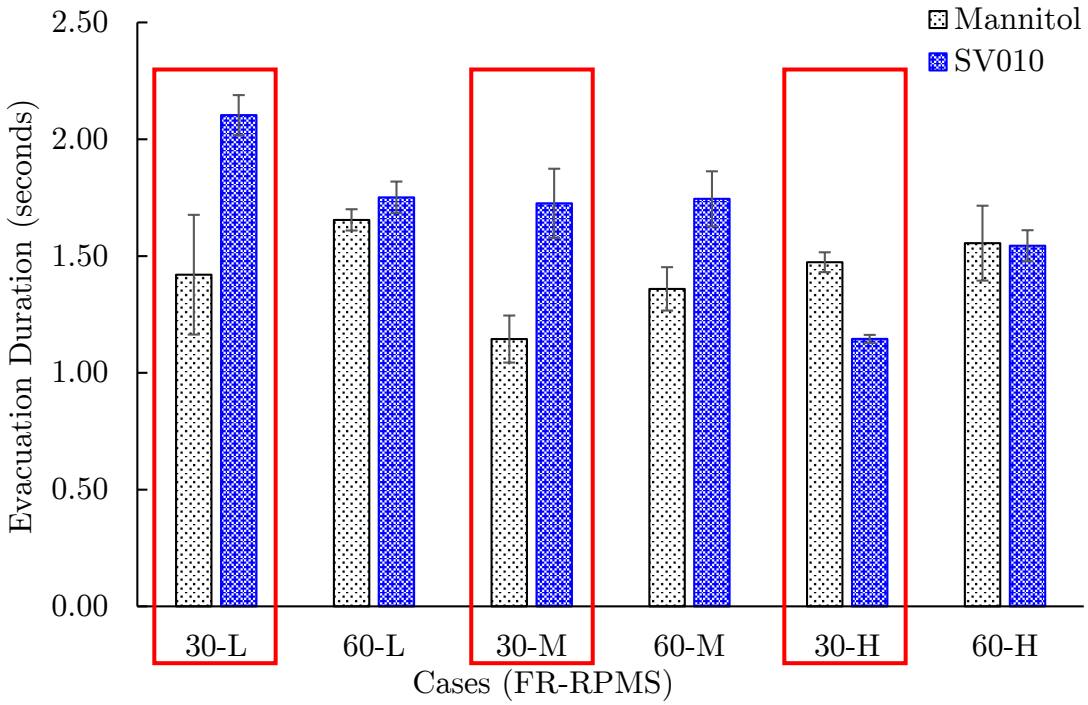

Figure 11: Duration of Observed Evacuation to 90% of the emission. Where identical flow conditions yield statistically significant duration for mannitol and SV010, a red box as has been drawn.

3.4 Correlation to Emitted Mass of Powder

The previous analysis provides information about the time variation in powder movement through the chosen FOV. To understand if this can be directly related to total mass emission behaviour, the light attenuation signals were integrated to obtain a value to describe the quantity of powder moving through the FOV. For mannitol, the integral of these time series signals shown in Appendix E (Figure E.23) was found to be highly correlated (0.95) to the total amount of powder emitted from the capsule as shown in Figure 12. However, this correlation did not hold for SV010. This could be due to an imaging limitation caused by SV010 particles being more likely to overlap and hence harder to image fully over the channel depth. While this can also occur for mannitol, it is less prevalent after the initial evacuation burst, likely due to blockage of the aperture. Additionally, for SV010, there is less of a bias towards the inline position; therefore, it is possible that a portion of the evacuated powder would occasionally fall outside the measured FOV. This is unlikely for mannitol which evacuates most strongly in line with the cross-flow (as demonstrated in Section E.0.1); therefore, it is logical to assume that the FOV would capture the majority of particles at a given instant in time.

Given the strong correlation of total mass with the integral of intensity signals for mannitol, the cumulative sum of the time series shown in Figures E.23, can be scaled by the total powder emission to obtain curves describing the emitted mass fraction from the capsule over time. Figure 13 shows this behaviour from the capsule for mannitol under all flow conditions.

For all cases, the mannitol experiences an initial burst of powder emission followed by a plateauing region for various amounts of time, as shown in Figure 13. For all cases evacuation was seen

to begin immediately following the initial rotation before reaching steady state speeds. To demonstrate how much powder evacuation has occurred during this acceleration, the time of powder evacuation was normalised by the rise-time of the capsule's rotation speed in Figure 13. Using this metric demonstrates how, by increasing the rotation speed, a greater portion of the initial evacuation burst will occur during the acceleration period rather than at a steady-state rotation speed. For the low rotation speed setting less than a quarter of the powder that would be emitted occur under capsule acceleration. For the medium and high rotation cases this increases to well over 50% of the mass evacuation occurring during the acceleration period followed by significantly reduced rate of evacuation as a result of powder packing over the lateral holes (Alfano et al. 2022).

Further studies are merited to understand this process further. However, this is beyond the scope of this particular contribution.

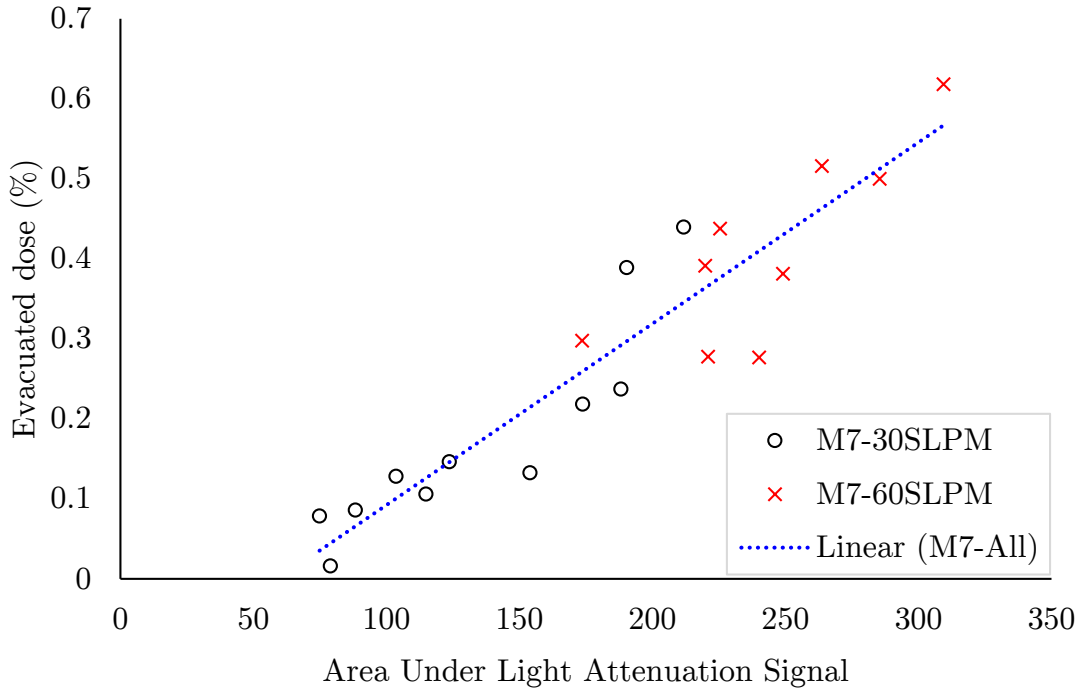

Figure 12: Correlation between the integral of the normalised light attenuation and total powder emission for mannitol. Correlation coefficient = 0.95

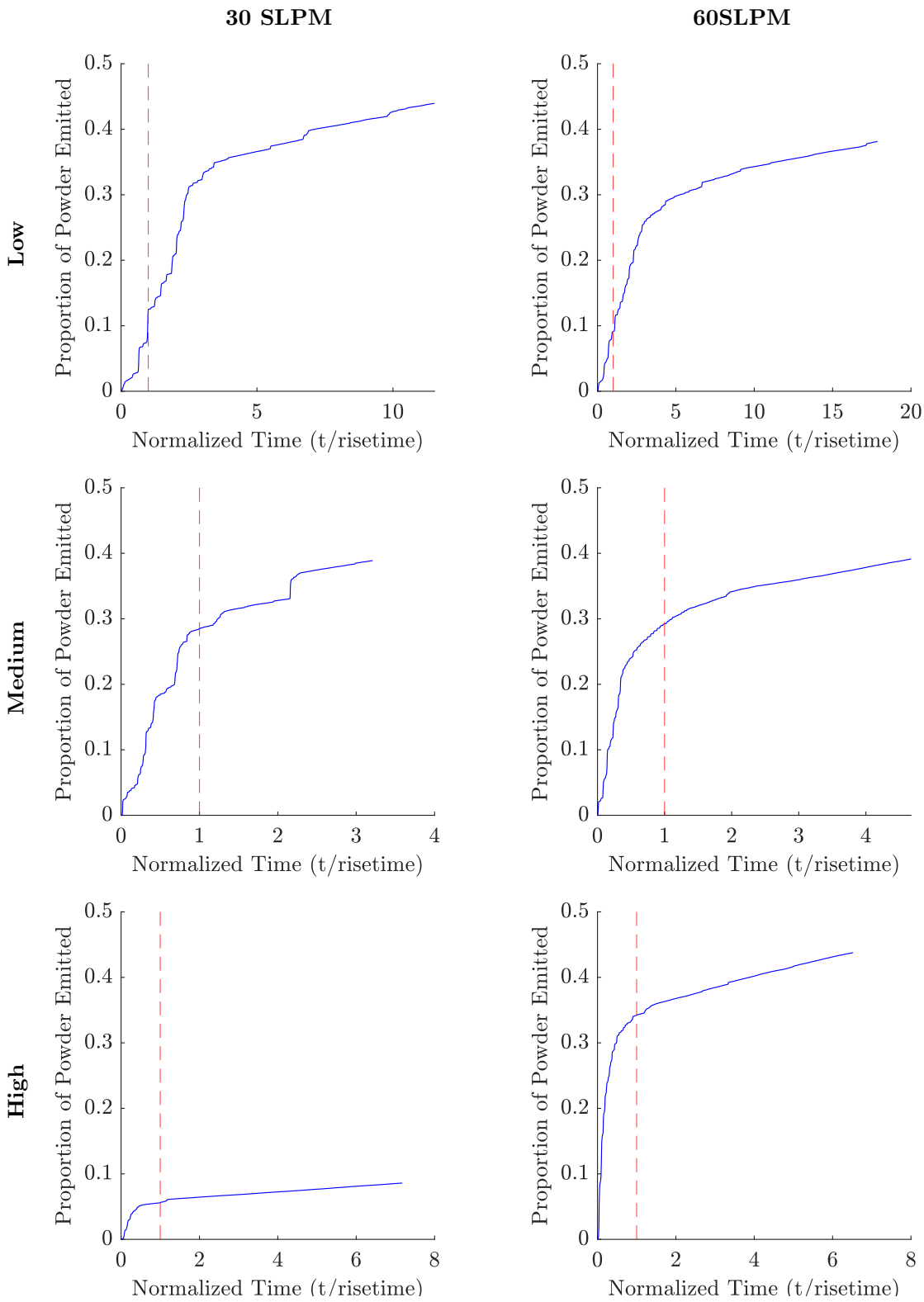

Figure 13: Powder evacuation over time for mannitol. Time normalised by rise time for rotation to reach steady state in each case.The dotted red line indicates when rotation has reached steady state.

The mass emission behaviour demonstrated in Figure 13 is similar to that which has been observed for capsule-based devices (Behara et al. 2011). Despite providing useful data for real-time analysis of evacuated powder mass under repeatable conditions of rotation speed and flow rate no clear mass emission patterns were observed. With a lack of any identifiable time-dependent behaviours that could differentiate different flow conditions, a statistical model was applied.

All the evacuation curves formed generally similar curve, therefore, a natural logarithmic function could be fitted to determine the rate of emptying *(a)* as per Equation 1. To ensure the function fit each curve and was a suitable descriptor of the data, the coefficient of determination R^2 was utilised (Behara et al. 2011). For each case the curve fit using Equation 1 and obtained an R^2 of at least 0.85.

$$EmittedDose = a \ln t + c \tag{1}$$

Figure 14 shows the correlation between the rate of emptying coefficient from the log model fit to the evacuation percentage. It is shown that the flow rate heavily drives the emptying rate through the capsule. This is consistent with observations of the powder emptying behaviour shown in Figure 6 whereby an increase in flow rate generated larger bursts of powder exiting the capsule.

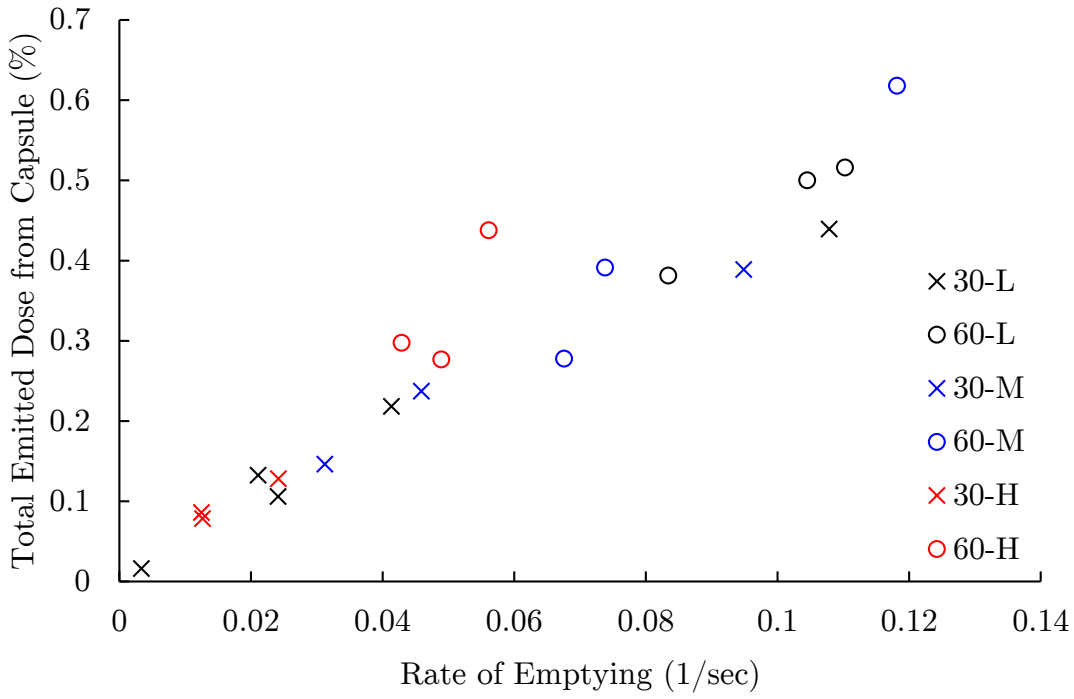

Figure 14: Rate of emptying *(a)* and total mannitol emitted from capsule.

3.5 Mannitol Powder Sizing

By measuring the particle size of mannitol as it exits the capsule an understanding of the degree of dispersion and deagglomeration can be developed. By analysing the PDF of aerodynamic diameter of the mannitol agglomerates, the effect of the evacuation mechanism on deagglomeration

can be seen. Figure F.26 shows a a high degree of similarity between all the mannitol cases regardless of flow rate or rotation speed. No significant difference in the distribution of particles by size band was found for all tested flow conditions.

The size distribution is repeatable regardless of the amount of powder evacuated which, as previously stated is highly variable. Figure 15 shows that a for each case a majority of the mannitol agglomerates are less than 50 μm in diameter as it exits the capsule. The lack of larger agglomerates and the consistency between different flow conditions suggests dispersion is overwhelmingly driven by shearing at the capsule aperture than than the turbulence or body forces acting due to rotation.

If the powder is mainly dispersed by shearing effects, this explains the observation of a longer evacuation time for 60 SLPM stated in Section 3.3. In typical DPI configurations, increasing flow rates is expected to decrease the evacuation time. However in this case the mannitol coverage of the aperture due to centrifugal force needs to be overcome by the cross flow. The increase in flow rate allows for this shearing force to be achieved and more powder is able to evacuate. Given the window of time the powder has where it is directly exposed to the air flow, more rotations are needed.

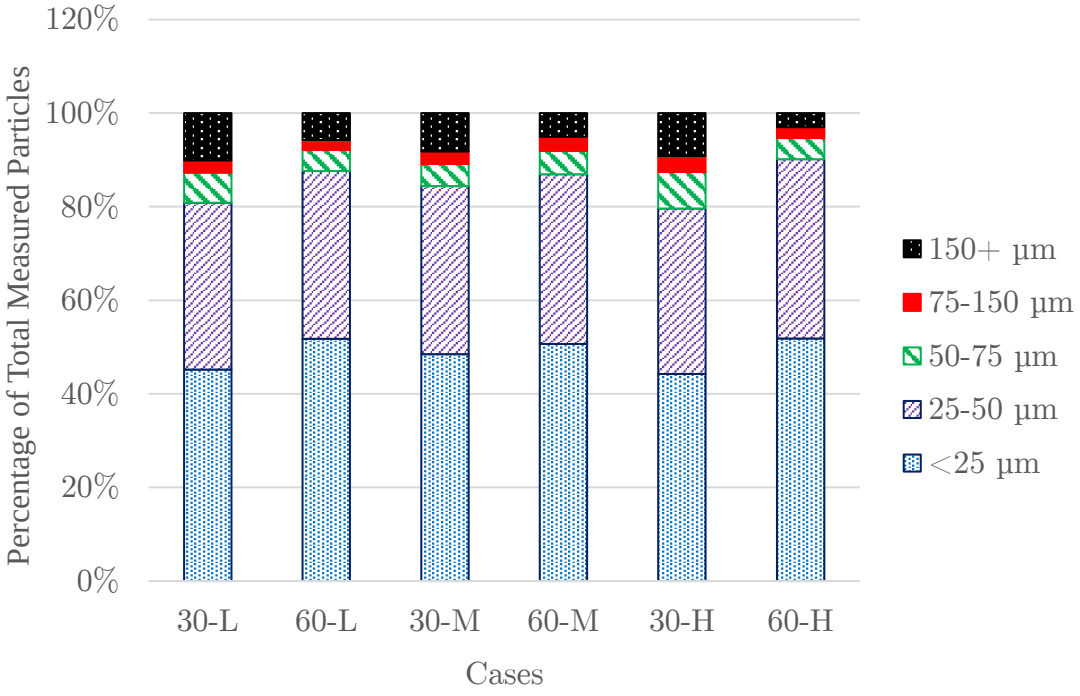

Figure 15: Proportion of Mannitol in each size band during capsule evacuation.

4 Summary and Conclusion

This experiment enabled the visualisation and measurement of powder as it exited a rotating capsule under coupled but separately controlled rotation speed and air flow conditions. Cohesion between powder particles heavily influenced the degree of powder evacuation from the capsule,

which decreased at higher rotation speeds for mannitol. Previous studies had emphasised the importance of centrifugal force in capsule evacuation, however for cohesive powders this has the potential to block the aperture and prevent further evacuation. In this experimental configuration, when capsule rotation is fixed about a certain axis without capsule collision, this aperture blockage cannot be mechanically dislodged and severely hinders capsule performance. This is an observation especially relevant to account for CFD studies, many of which do not account for the role of capsule collisions.

Previous works have often stated the importance of predictable/repeatable capsule motion being responsible for consistent evacuation(Behara et al. 2011) and the dispersion as measured by fine particle fraction was proportional to flow rate (Tang et al. 2023). However, in these works, the capsules were free to collide with chamber walls. This collision process has been known to improve dispersion through impaction between the particles and the moving capsule(Benque and Khinast 2019). For the experiment presented in this paper, the collision mechanics are eliminated and we show only the effect of forces due to rotation and air flow directed through the capsule.

The mass of powder evacuated was highly variable even with repetitions of near identical flow and rotation conditions in a highly controlled environment demonstrating the role of powder properties within the capsule and the arrangement of agglomerates prior to device actuation. A summary of key findings are stated below:

1. For cohesive powder, increasing rotation speed worsened evacuation performance and shortened the duration of evacuation due to early blockage.
2. Evacuation of mannitol (relating to total emitted mass) is heavily influenced by the degree of agglomeration and arrangement of powder within the capsule. As a result, identical flow conditions/rotation speeds can yield largely different results
3. For mannitol, the duration of evacuation is longer at 60 SLPM compared to 30SLPM, but this is not the case for SV010 due to the lack of cohesion blocking aperture thus slowing the evacuation process
4. Non-cohesive powders are able to evacuate more continuously but both powders experience periodic behaviour in evacuation when capsule/flow alignment is achieved.
5. Powder evacuation over time for mannitol can be described using a natural log function whereby the rate of emptying is proportional to the emitted dose.
6. A majority of mannitol evacuation occurs while the capsule is accelerating. Therefore, assumptions of constant rotation speed may not necessarily represent the forces experienced by powder within rotating capsules.
7. The size distribution of mannitol as it evacuates the capsule is largely consistent for all flow/rotation cases. Dispersion appears to be driven by shearing at the capsule aperture.

While this study does not directly emulate commercial devices the behaviours observed due to rotation and airflow interaction can be used to form a foundational understanding of the variables in capsule based devices.

5 Funding statement

This work was funded by the Australian Research Council under Grant Number LP190100842.

6 Disclosure statement

The authors report there are no competing interests to declare.

References

Alfano, Francesca Orsola et al. (Dec. 2022). 'DEM analysis of powder deaggregation and discharge from the capsule of a carrier-based Dry Powder Inhaler'. In: *Advanced Powder Technology* 33.12, p. 103853. ISSN: 0921-8831. DOI: 10.1016/j.apt.2022.103853. URL: https://www.sciencedirect.com/science/article/pii/S0921883122004320.

Almeida, Lucilla C. et al. (Aug. 2022). 'Capsule-Based dry powder inhaler evaluation using CFD-DEM simulations and next generation impactor data'. en. In: *European Journal of Pharmaceutical Sciences* 175, p. 106226. ISSN: 09280987. DOI: 10.1016/j.ejps.2022.106226. URL: https://linkinghub.elsevier.com/retrieve/pii/S0928098722001117.

Azeem, Athiya et al. (Jan. 2023). 'Quantifying Agglomerate-to-Wall Impaction in Dry Powder Inhalers'. en. In: *Pharmaceutical Research* 40.1, pp. 307–319. ISSN: 0724-8741, 1573-904X. DOI: 10.1007/s11095-022-03446-0. URL: https://link.springer.com/10.1007/s11095-022-03446-0.

Behara, Srinivas Ravindra Babu et al. (Nov. 2011). 'Kinetics of emitted mass—A study with three dry powder inhaler devices'. en. In: *Chemical Engineering Science* 66.21, pp. 5284–5292. ISSN: 00092509. DOI: 10.1016/j.ces.2011.07.029. URL: https://linkinghub.elsevier.com/retrieve/pii/S000925091100491X.

Benque, Benedict and Johannes G. Khinast (Aug. 2019). 'Understanding the motion of hard-shell capsules in dry powder inhalers'. en. In: *International Journal of Pharmaceutics* 567, p. 118481. ISSN: 03785173. DOI: 10.1016/j.ijpharm.2019.118481. URL: https://linkinghub.elsevier.com/retrieve/pii/S037851731930523X.

Chaurasiya, Birendra and You-Yang Zhao (Dec. 2020). 'Dry Powder for Pulmonary Delivery: A Comprehensive Review'. In: *Pharmaceutics* 13.1, p. 31. ISSN: 1999-4923. DOI: 10.3390/pharmaceutics13010031. URL: https://www.ncbi.nlm.nih.gov/pmc/articles/PMC7824629/.

Claus, Sarah et al. (Jan. 2014). 'How can we bring high drug doses to the lung?' en. In: *European Journal of Pharmaceutics and Biopharmaceutics* 86.1, pp. 1–6. ISSN: 09396411. DOI: 10.1016/j.ejpb.2013.11.005. URL: https://linkinghub.elsevier.com/retrieve/pii/S0939641113003779.

Coates, Matthew S. et al. (June 2005). 'The Role of Capsule on the Performance of a Dry Powder Inhaler Using Computational and Experimental Analyses'. en. In: *Pharmaceutical Research* 22.6, pp. 923–932. ISSN: 0724-8741, 1573-904X. DOI: 10.1007/s11095-005-4587-y. URL: http://link.springer.com/10.1007/s11095-005-4587-y.

Ding, Li et al. (Aug. 2021). 'A Quality by Design Framework for Capsule-Based Dry Powder Inhalers'. en. In: *Pharmaceutics* 13.8, p. 1213. ISSN: 1999-4923. DOI: 10.3390/pharmaceutics13081213. URL: https://www.mdpi.com/1999-4923/13/8/1213.

Goh, Hui Ping, Paul Wan Sia Heng and Celine Valeria Liew (Aug. 2018). 'Comparative evaluation of powder flow parameters with reference to particle size and shape'. In: *International Journal of Pharmaceutics* 547.1, pp. 133–141. ISSN: 0378-5173. DOI: 10.1016/j.ijpharm.2018.05.059. URL: https://www.sciencedirect.com/science/article/pii/S0378517318303661.

Huynh, B. K. et al. (Oct. 2015). 'An Investigation into the Powder Release Behavior from Capsule-Based Dry Powder Inhalers'. en. In: *Aerosol Science and Technology* 49.10, pp. 902–911. ISSN: 0278-6826, 1521-7388. DOI: 10.1080/02786826.2015.1082532. URL: http://www.tandfonline.com/doi/full/10.1080/02786826.2015.1082532.

Islam, Nazrul and Matthew J. Cleary (May 2012). 'Developing an efficient and reliable dry powder inhaler for pulmonary drug delivery – A review for multidisciplinary researchers'. en. In: *Medical Engineering Physics* 34.4, pp. 409–427. ISSN: 13504533. DOI: 10.1016/j.medengphy.2011.12.025. URL: https://linkinghub.elsevier.com/retrieve/pii/S1350453312000033.

Lavorini, Federico, Massimo Pistolesi and Omar S. Usmani (May 2017). 'Recent advances in capsule-based dry powder inhaler technology'. en. In: *Multidisciplinary Respiratory Medicine* 12.1, p. 11. ISSN: 2049-6958. DOI: 10.1186/s40248-017-0092-5. URL: https://doi.org/10.1186/s40248-017-0092-5.

Li, L.J. et al. (Aug. 2022). 'DEM modelling of breakage behaviour of semi-brittle agglomerates subject to compaction and impaction'. en. In: *Powder Technology* 408, p. 117710. ISSN: 00325910. DOI: 10.1016/j.powtec.2022.117710. URL: https://linkinghub.elsevier.com/retrieve/pii/S0032591022006039.

Lowe, A. et al. (Apr. 2021). 'Erratum to "Fragmentation dynamics of single agglomerate-to-wall impaction" [Powder Technology 378 (2021) 561–575, DOI: 10.1016/j.powtec.2020.10.021]'. en. In: *Powder Technology* 382, p. 262. ISSN: 00325910. DOI: 10.1016/j.powtec.2020.12.048. URL: https://linkinghub.elsevier.com/retrieve/pii/S0032591020312158.

Mahmoudi, S. et al. (May 2019). 'Fluidisation characteristics of lactose powders in simple turbulent channel flows'. en. In: *Experimental Thermal and Fluid Science* 103, pp. 201–213. ISSN: 08941777. DOI: 10.1016/j.expthermflusci.2019.01.012. URL: https://linkinghub.elsevier.com/retrieve/pii/S0894177718315954.

Martinelli, Francesco et al. (June 2015). '"Pierce and inhale" design in capsule based dry powder inhalers: Effect of capsule piercing and motion on aerodynamic performance of drugs'. en. In: *International Journal of Pharmaceutics* 487.1–2, pp. 197–204. ISSN: 03785173. DOI: 10.1016/j.ijpharm.2015.04.003. URL: https://linkinghub.elsevier.com/retrieve/pii/S0378517315003105.

Newman, S.P. and W.W. Busse (May 2002). 'Evolution of dry powder inhaler design, formulation, and performance'. en. In: *Respiratory Medicine* 96.5, pp. 293–304. ISSN: 09546111. DOI: 10.1053/rmed.2001.1276. URL: https://linkinghub.elsevier.com/retrieve/pii/S0954611101912764.

Shur, Jagdeep et al. (Dec. 2012). 'Effect of Device Design on the In Vitro Performance and Comparability for Capsule-Based Dry Powder Inhalers'. en. In: *The AAPS Journal* 14.4, pp. 667–676. ISSN: 1550-7416. DOI: 10.1208/s12248-012-9379-9. URL: http://link.springer.com/10.1208/s12248-012-9379-9.

Singh, Gajendra, Albyn Lowe et al. (Oct. 2021). 'Effect of inflow conditioning for dry powder inhalers'. en. In: *International Journal of Pharmaceutics* 608, p. 121085. ISSN: 03785173. DOI: 10.1016/j.ijpharm.2021.121085. URL: https://linkinghub.elsevier.com/retrieve/pii/S0378517321008917.

Singh, Gajendra, Patricia Tang et al. (Mar. 2022). 'From laminar to turbulent flow in a dry powder inhaler: The effect of simple design modifications'. en. In: *International Journal of Pharmaceutics* 616, p. 121556. ISSN: 03785173. DOI: 10.1016/j.ijpharm.2022.121556. URL: https://linkinghub.elsevier.com/retrieve/pii/S0378517322001107.

Tang, Patricia et al. (July 2023). 'The role of capsule aperture size on the dispersion of carrier-based formulation at different air flowrates'. en. In: *International Journal of Pharmaceutics* 642, p. 123152. ISSN: 03785173. DOI: 10.1016/j.ijpharm.2023.123152. URL: https://linkinghub.elsevier.com/retrieve/pii/S0378517323005720.

Zhu, Qixuan et al. (Nov. 2023). 'CFD-DEM investigation of the effects of aperture size for a capsule-based dry powder inhaler'. en. In: *International Journal of Pharmaceutics* 647, p. 123556. ISSN: 03785173. DOI: 10.1016/j.ijpharm.2023.123556. URL: https://linkinghub.elsevier.com/retrieve/pii/S0378517323009778.

A Methodology Supplementary Material

A.1 Powder Selection

The mannitol powder was produced using a spray drier (Buchi 290) using the following parameters: Air Inlet Temperature of 160°C, atomising air rate of 60 mL/h and maximum aspiration set to 38 m^3/h and a feed-rate of 14.75 mL/min and feed concentration of 150 g/L. Under these conditions the approximate powder size achieved was 7 μm where $d_{50} = 6.92\mu m$ and a span of 1.28 μm.

Previous studies that have examined emission rate have typically used carrier-dominated blends with fines. However, the powder in this study was chosen to both be in line with previous works (Azeem et al. 2023; Singh, Tang et al. 2022; Singh, Albyn Lowe et al. 2021) and to isolate evacuation behaviour as it related to constituent side. To better understand how agglomeration factors into emission behaviour direct imaging of the powder was used to size agglomerates immediately downstream of the capsule.

The powder was loaded into the device inside preweighed gelatin capsules. The capsule were stored in a airtight container in ambient conditions until used. Powder was stored in a separate airtight container with desiccant beads to prevent agglomeration due to humidity.

A.2 Imaging

The experiment imaging apparatus is shown below in Figure A.16. The laser was used to generate a beam with a wavelength of 808 nm, which could then be diffused and collimated to back-light the particles in the channel for microscopic imaging. For far field imaging a flood light was utilised in place of the laser.

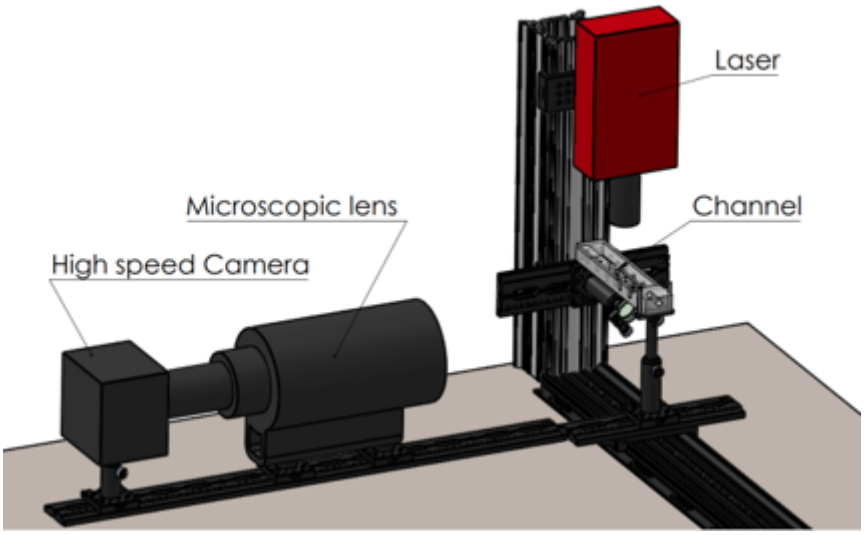

Figure A.16: Full Imaging apparatus and Experimental schematic

B Qualitative Evacuation Time Series

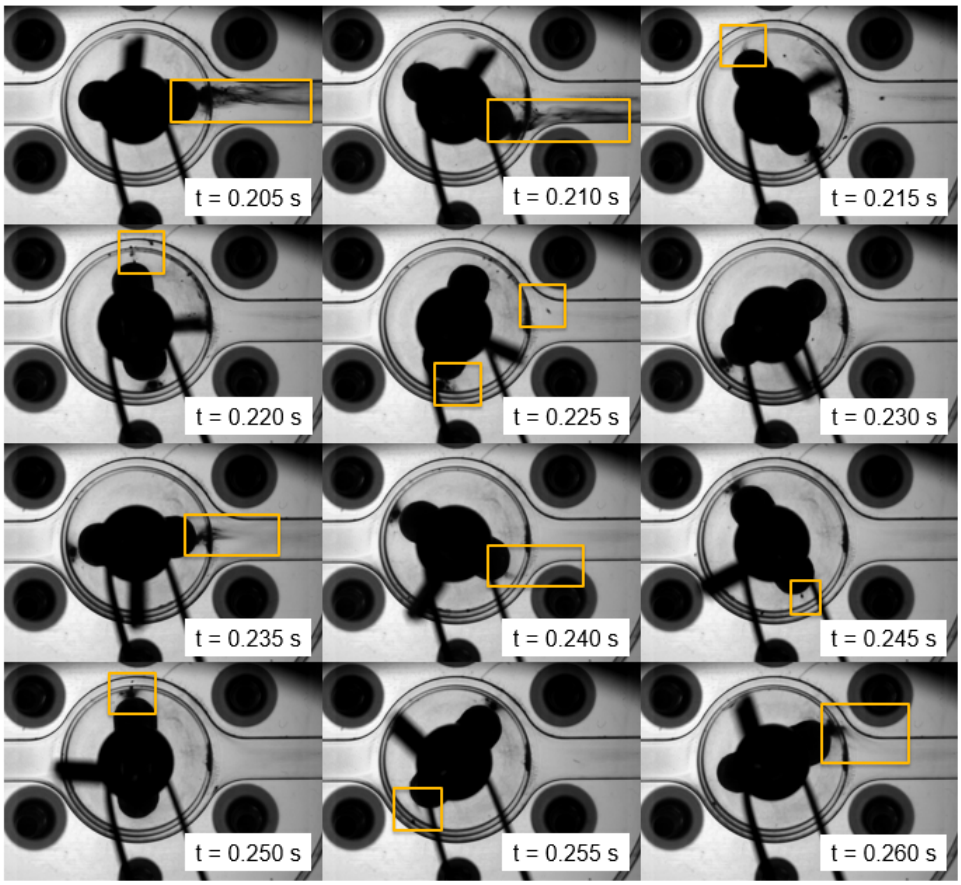

Figure B.17: Far Field Imaging of Mannitol evacuation from capsule with low rotation speed and 60 SLPM.

C Rotation Speed Measurements

Three rotation speeds were chosen for this study. The degree of fluctuation was quantified for each case and shown below in Figure C.18

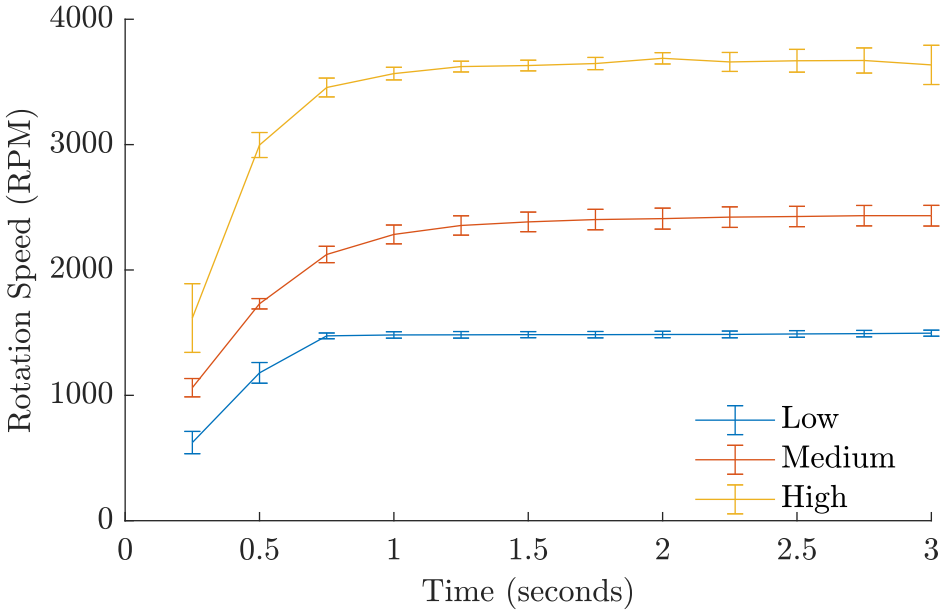

Figure C.18: Time Averaged Rotation Speed Measurement.

In order to obtain these measurements of rotation speed in rotation speed and acceleration time of the capsule, a real time monitoring system was required. To achieve this a 3D printed plastic fin was attached to the shaft of the rotating platform below the drive belt. This fin is visible in Figure C.19 and was used to interrupt a laser path from a low powder diode to a photoresistor as the platform rotated as shown in Figure C.20. The sensor was connected to an Analog Input module (National Instruments NI9215) sampling at 2kHz. This signal was then processed in Matlab using peak picking functions to measure the rotation speed.

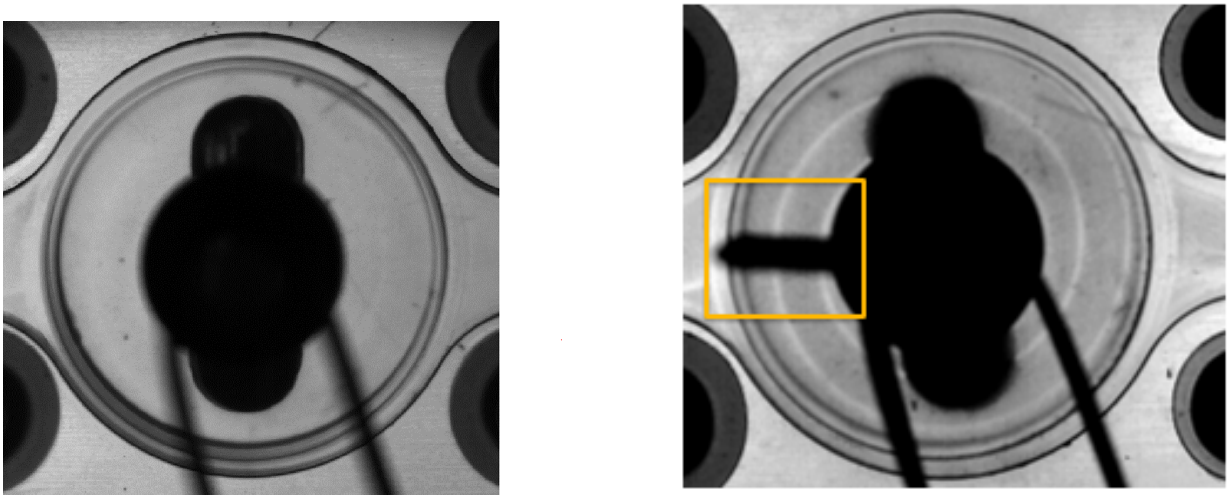

(a) without Fin (b) With Fin

Figure C.19: Capsule on rotating bed with and without 3D printed fin.

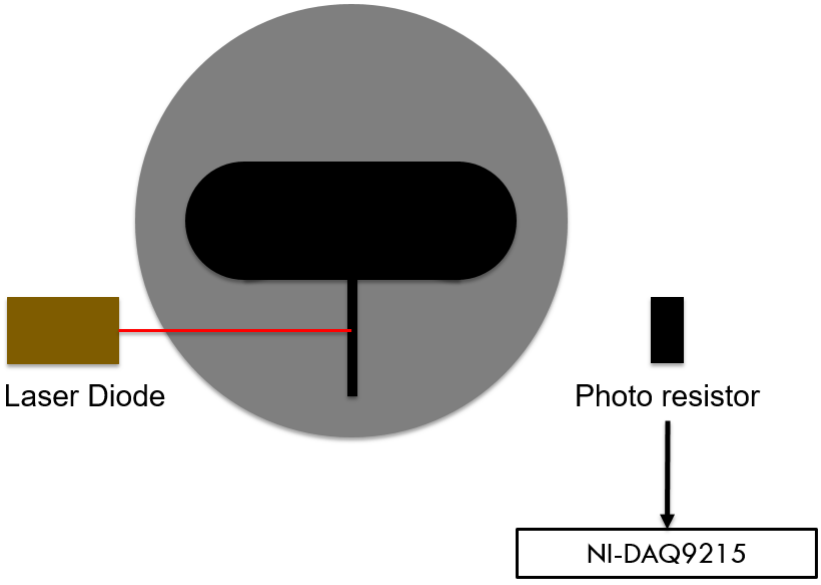

Figure C.20: Rotation Speed measurement system

D Signal Processing

The light attenuation signals shown in Section 3.3 and Appendix E were obtained by processing the high-speed microscopic images taken downstream of the capsule. From these images, the total light intensity of the image was determined as the sum of the total pixel intensity for a given image. This was done for every image in the sequence until a overall light attenuation signal over time was generated. This raw signal however could not be compared between cases due to two key factors that had to be corrected for.

Firstly, the starting light intensity was a direct result of the laser strength; any movement of the laser or warming up over the day could cause differences in the starting intensity. Any subsequent changes due to the presence of powder would be compared to this background. To correct for this the signal was first normalised by the maximum intensity (the background).

The signal was then inverted so that the peaks (rather than troughs) would be indicative of particle movement throughout the FOV. This also provides further clarity in metrics around the integral of the normalized light attenuation signal.

Secondly, wall deposition is a common limitation of imaging techniques for cohesive powders like mannitol. To mitigate this issue, a moving minimum was subtracted from the signal to identify only movement in and out of the frame.

This final signal could then be analysed to compare different cases. The stages of this signal processing are shown in Figure D.21

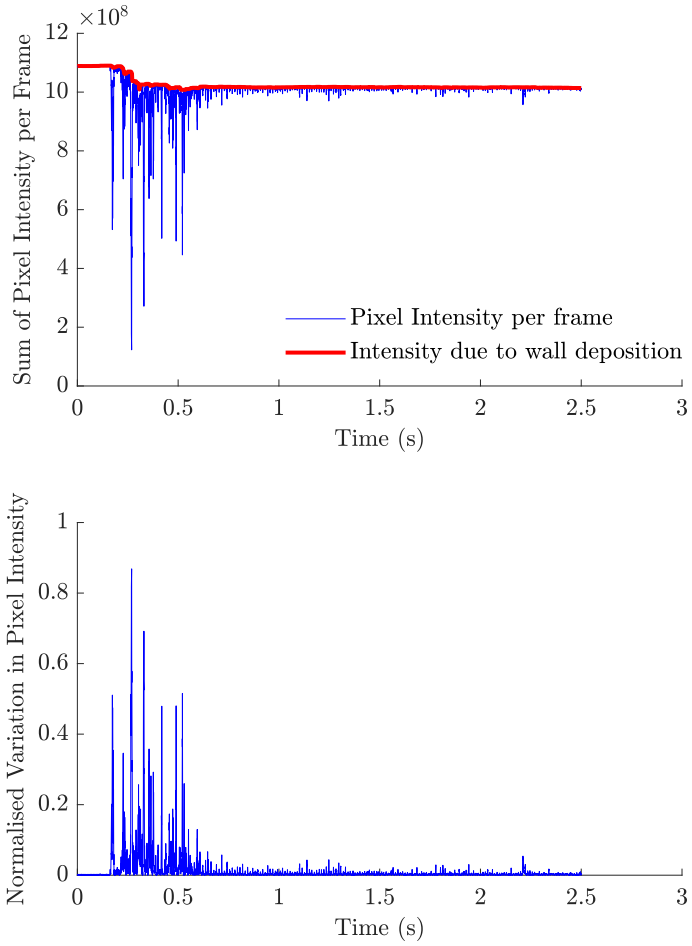

Figure D.21: Sample Signal Processing for Mannitol 30 SLPM Low rotation speed.

E Pixel Intensity

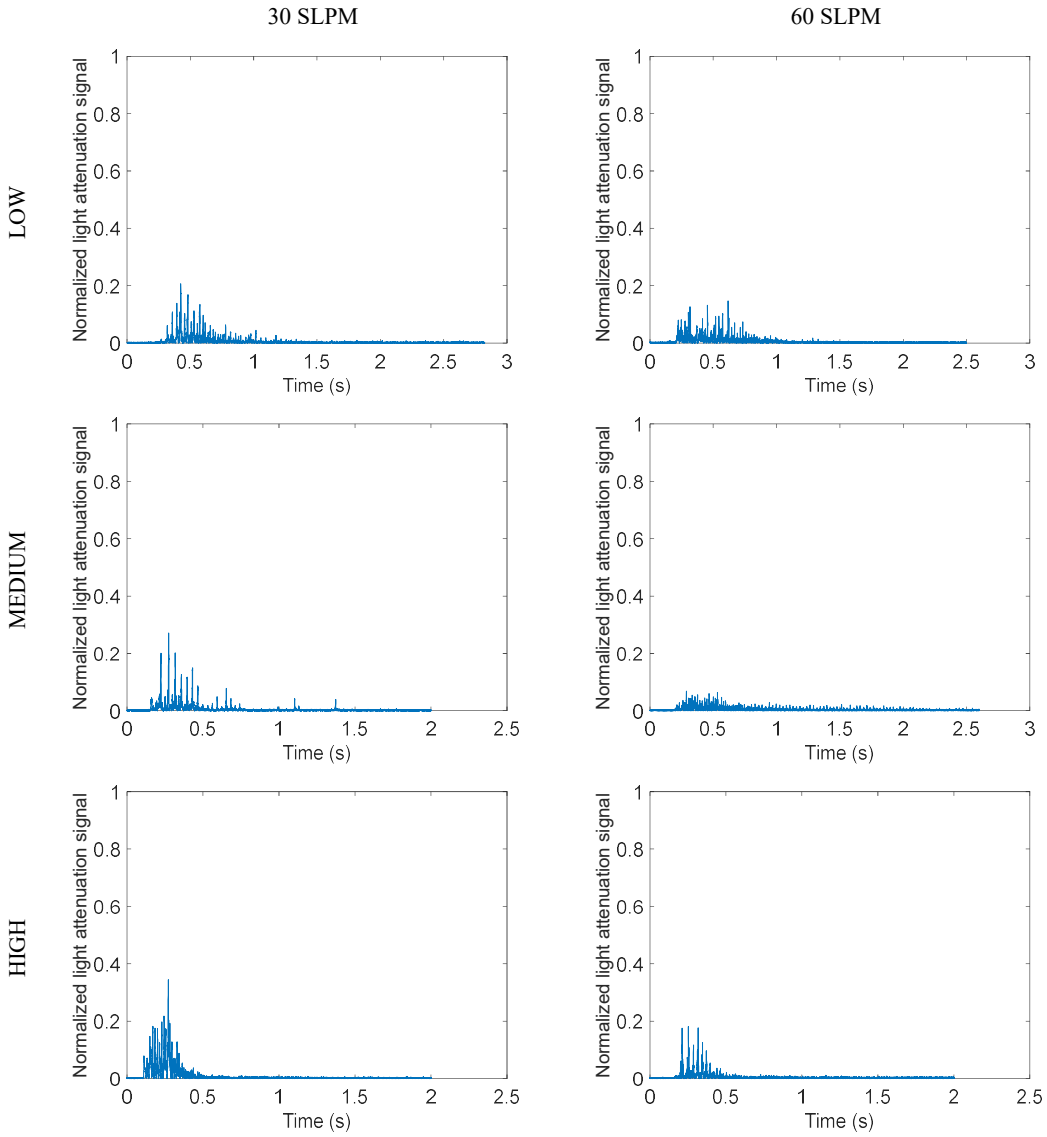

Figure E.22: Light attenuation of powder for SV010 at downstream of capsule FOV.

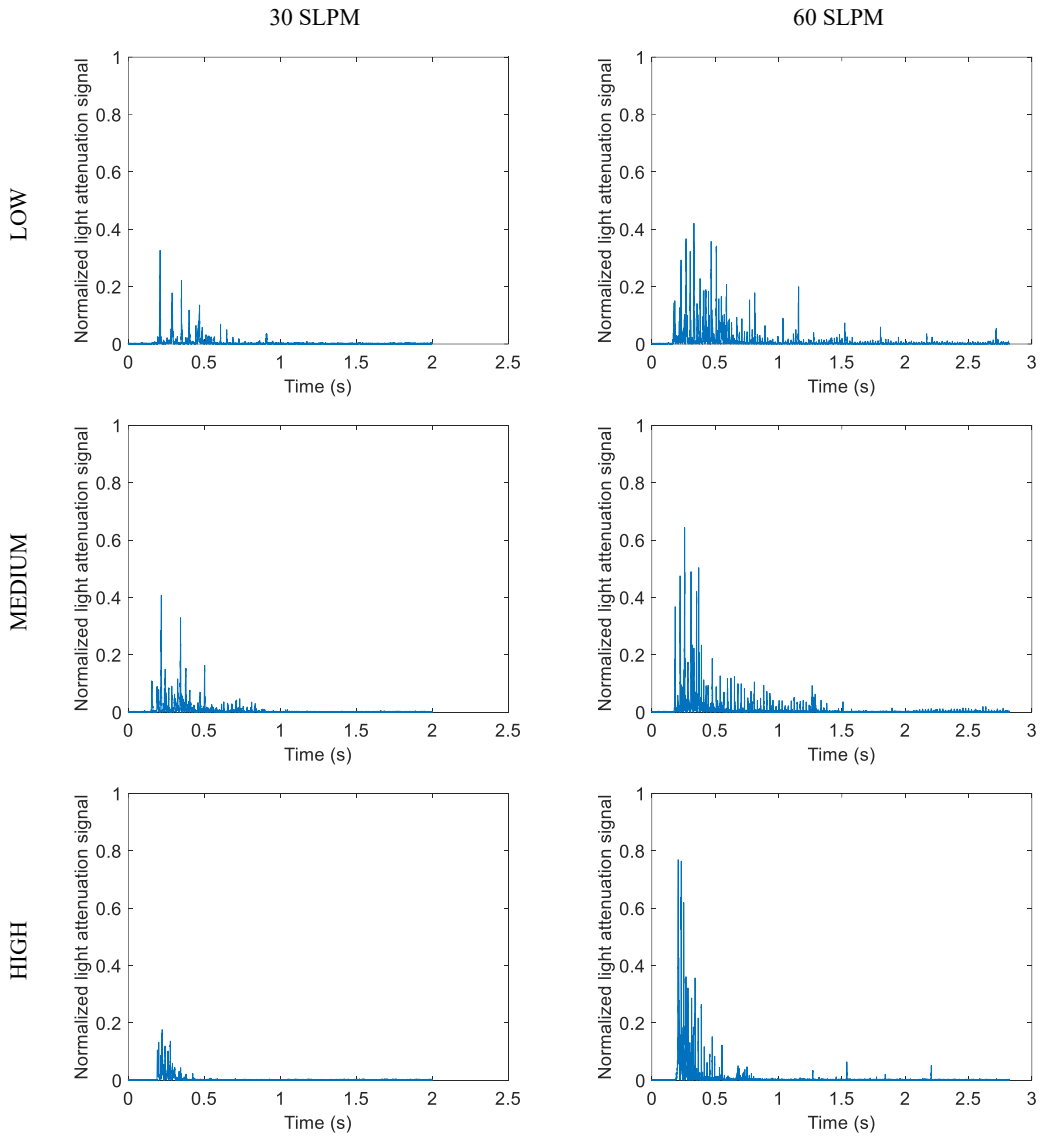

Figure E.23: Light attenuation of powder for Mannitol at downstream of capsule FOV.

E.0.1 Analysis of Periodic Behaviour

As previously mentioned powder emission signals such as those shown in Figures E.22 and E.23 demonstrate periodic emissions. The following considers a frequency analysis of the evacuation behaviour.

When observing powder evacuation qualitatively, the lactose carrier appeared to evacuate more continuously with fewer periods of discontinuity as shown in Figure 10, in contrast to mannitol. Upon analysis of the light attenuation signals, both powders exhibit period behaviour that can be attributed to the capsule aperture alignment with the oncoming flow that enhances the overall evacuation.

This period behaviour is most easily identified by conducting a Fast Fourier Transform (FFT) of

the light attenuation signals. his technique has previously been utilised in literature to describe powder fluidisation behaviour (Mahmoudi et al. 2019). The application of an FFT converts the time series signal into the frequency domain and shows consistent patterns in the light variation that correspond to powder evacuation behaviour. Prior to the FFT, Hamming windowing was applied to the signal such that only continuous sections of data were included.

For all mannitol cases, the only distinct pattern that appeared between repetitions was for the Low rotation speed at 60 SLPM. In this case, the intensity peaks occurred at integer multiples of the rotation frequency (approximately Low: 25 Hz, Medium: 41.7 Hz and High: 60.8 Hz) as shown in Figure E.24. This is consistent with the qualitative assessment of capsule evacuation where large bursts tend to correlate with the capsule alignment to the flow. For a low RPM rate where centrifugal forces are low, the 60SLPM case strongly favours evacuation when the capsule is in line with the flow. At other angles, airflow through the capsule is significantly reduced, and with minimal evacuation due to centrifugal force, this correlation to rotation speed is most identifiable under this condition.

The lactose carriers are uninhibited by cohesion as they evacuate from the capsule and therefore can evacuate in a continuous manner even when the capsule is not in line with the air flow. As a result, whilst frequency peaks are still evident for SV010, they are broader than those shown for mannitol, as observed when comparing the peaks in Figure E.24 to Figure E.25. This broadness indicates a broader range of phenomena contributing to the evacuation of the powder instead of just a capsule alignment event. While these peaks are somewhat aligned with the rotation frequency, they are also broader and more variable between repetitions, suggesting a variety of time-dependent emptying behaviours.

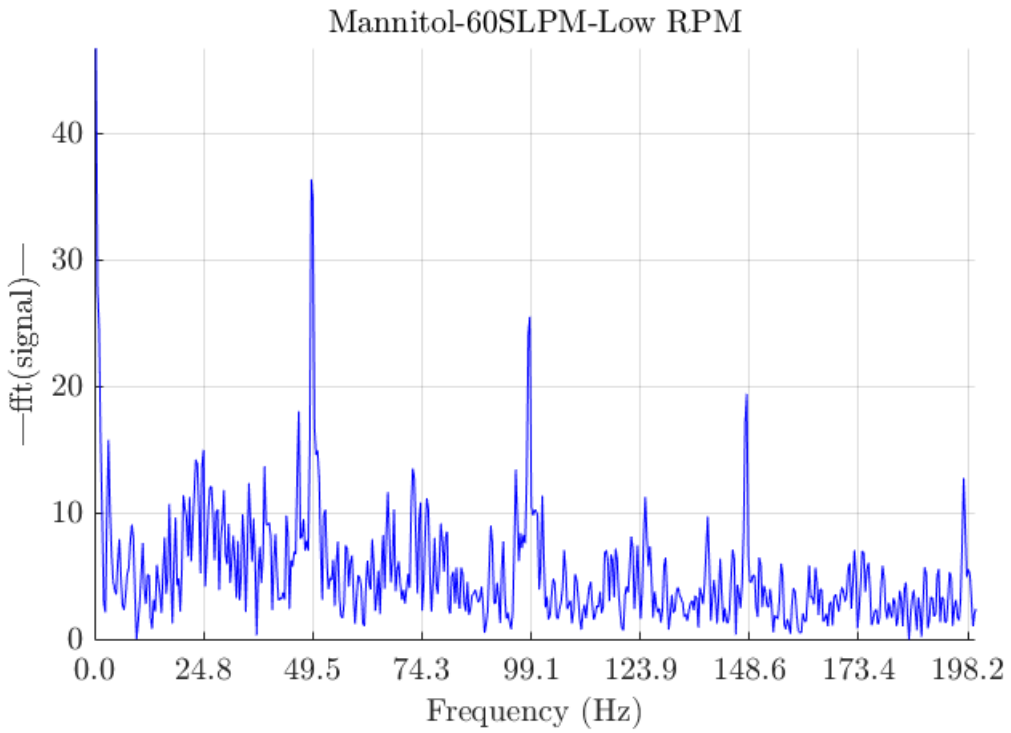

Figure E.24: FFT of light attenuation signals for Mannitol at 60 SLPM and a steady state rotation speed of 1484 RPM (24.8 Hz)

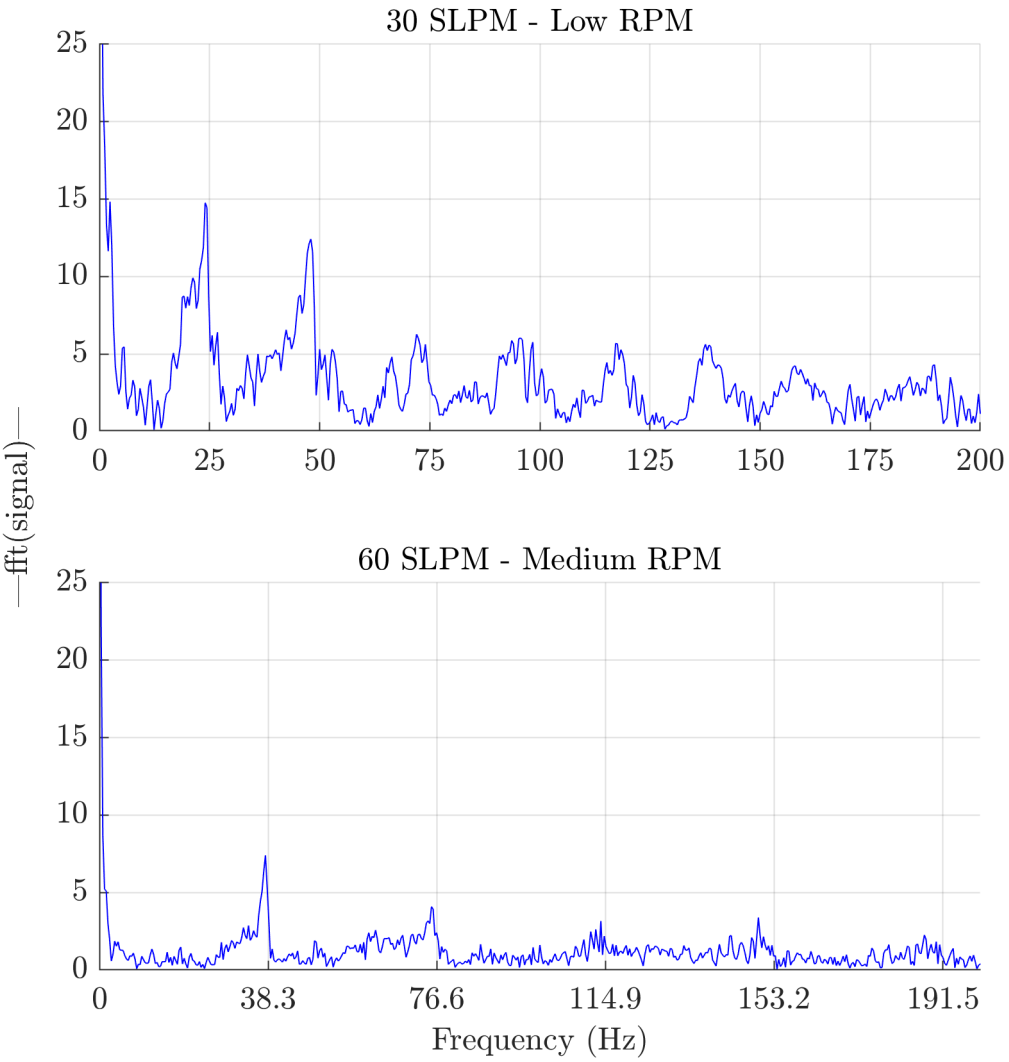

Figure E.25: FFT for Light attenuation of select SV010 cases. Grid lines indicate multiples of the rotation speed. (25Hz and 38.3 Hz for Low and Medium RPM respectively)

F Mannitol Agglomerate Sizing

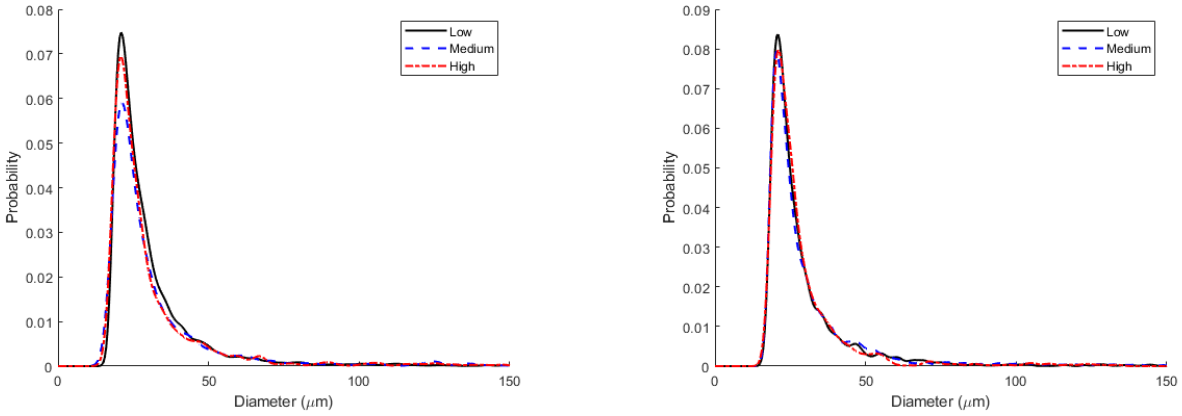

(a) (b)

Figure F.26: Size distribution of Mannitol at two flow rates